Mineralium Deposita
https://doi.org/10.1007/s00126-025-01361-z

INVITED PAPER

Granite-pegmatite-related gold skarns and associated Li-Cs-Ta pegmatites in the Archean Yilgarn Craton, Western Australia

Andreas G. Mueller[1]

Received: 30 October 2024 / Accepted: 18 March 2025

Abstract

In greenstones of the east-central Yilgarn Craton, Western Australia, Li-Cs-Ta (LCT) pegmatites of the albite-spodumene type (resources > 300 Mt at 1.4% Li_2O) are spatially associated with high-T (650–450 °C) granite-pegmatite-related skarn and skarn-quartz vein Au-Ag deposits (production 580 t Au). U-Pb and Rb-Sr ages (2.65–2.62 Ga) link both the LCT pegmatites and gold deposits to a suite of peraluminous I-type biotite granites, magnetite-series in least-fractionated K-feldspar megacrystic members, and magnetite- or ilmenite-series in pegmatitic garnet-muscovite intrusions contaminated by melt interaction with continental crust. The granite-pegmatite complexes and the gold skarns formed at 11–15 km crustal depth (300–400 MPa) in a post-orogenic batholith environment at the margin of the 2.7 Ga Eastern Goldfields orogen. Gold occurs in both endo- and exoskarn, and in granite and pegmatite dikes. Calcite carbon isotopes, and initial $^{87}Sr/^{86}Sr$ ratios in scheelite relate the skarns to post-orogenic intrusions. Inner calcite, pyroxene, and outer biotite, cordierite, amphibole, and olivine impart a CO_2-Ca-Mg-K metasomatic signature to the hydrothermal system (e.g., Nevoria, Yilgarn Star, Copperhead). An exception is the Ghost Crab deposit, where anthophyllite, cummingtonite, and albite are major constituents in sodic gold ore replacing paragneiss in a zone of magnesian skarn. This deposit is proximal to the albite-spodumene pegmatites of the Mt Marion mine. The skarns in the Yilgarn Craton share the granite-pegmatite association, the gangue mineralogy, the Au-Bi-W geochemical signature, and low- to moderate salinity H_2O-CO_2 fluid inclusions with reduced tungsten skarns, and with world-class gold deposits in other Archean cratons (Kaapvaal, Slave, Superior, Dharwar).

Keywords Archean · LCT pegmatites · Au skarns · I-type granites

Introduction

Skarn deposits in the 3.0 Ga Southern Cross greenstone belt, Yilgarn Craton, Western Australia, produced more than 360 t gold (> 12 Moz; 1887–2024), whereas the total of skarn and skarn-quartz-vein deposits at the southwest margin of the 2.7 Ga Eastern Goldfields (EG) orogen amounts to 219 t gold (1894–2013). The calc-silicate deposits are spatially associated with 2.65–2.62 Ga I-type granites. Granite and pegmatite dikes are exposed in about 70% of all mines, and thick intrusions at up to 800 m depth caused the cessation of mining in three deposits (> 31 t Au) of the Southern Cross district.

In this study, we review the regional setting and chronological database of late- to post-orogenic granites associated with gold skarns and LCT pegmatites in the east-central Yilgarn Craton (Fig. 1). At first, emphasis is placed on the Southern Cross area, where the discovery of the Earl Grey spodumene pegmatite (189 Mt at 1.5% Li_2O; Phelps-Barber et al. 2022) below open pits mined for gold triggered renewed exploration. Mineralogical and metasomatic changes in the Nevoria gold skarn system and its coeval pegmatite-granite complex (Mueller et al. 2004) are integrated with new chemical data on Ca-Mg-CO_2 metasomatism in the source-distal Copperhead deposit. Petrogenetic grids and thermodynamic calculations using the electron probe micro-analyses (EPMA) of anthophyllite/chlorite-cordierite assemblages in the outer alteration zones of gold deposits provide constraints on the PT-conditions of skarn formation. We then describe granite-pegmatite-related gold skarn deposits in the Mt Marion-Wattle Dam and Pioneer Dome Au-Li ± Cs districts at the southwest margin of the

Editorial handling: B. Lehmann

✉ Andreas G. Mueller
andreas.mueller2@partner.kit.edu

1 Karlsruhe Institute of Technology, Applied Geosciences, Adenauerring 20b, D-76131 Karlsruhe, Germany

Published online: 16 April 2025

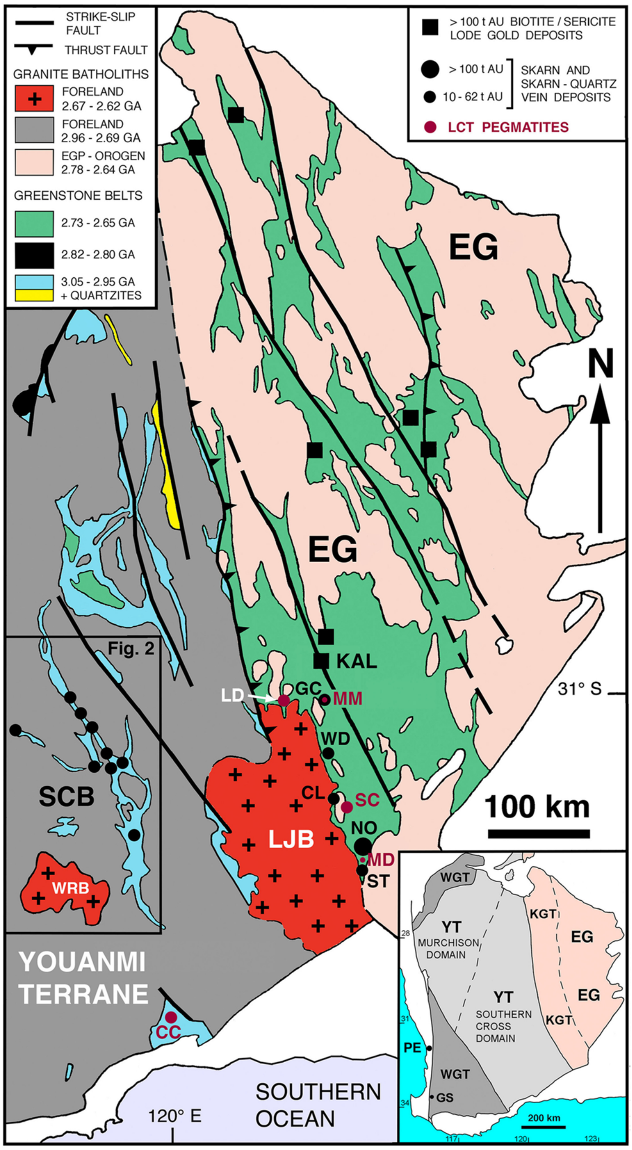

Fig. 1 Geologic map of the eastern Yilgarn Craton showing the 2.7 Ga Eastern Goldfields (EG) orogen and its continental foreland. (modified from Mueller et al. 2020). Regional faults in the orogen control mesothermal gold deposits (KAL=Kalgoorlie, 2000 t Au). In the Youanmi foreland, late- to post-orogenic I-type granites represented by the Wave Rock (WRB) and Lake Johnston batholiths (LJB) are associated with LCT pegmatites and gold skarn deposits in the Southern Cross greenstone belt (SCB), and with skarn and skarn-quartz vein deposits in the Kalgoorlie Terrane: Ghost Crab (GC), Wattle Dam (WD), Chalice (CL), Norseman (NO), and Scotia (ST). LCT pegmatite mines: Cattlin Creek (CC), Mount Deans (MD), Londonderry (LD), Mt Marion (MM), and Sinclair (SC). The inset map shows the subdivision of the craton into the EG orogen (KGT=Kalgoorlie Terrane), the Youanmi Terrane (YT), and the Western Gneiss Terranes (WGT). Note the Greenbushes LCT pegmatite (GS) south of Perth (PE). Coordinates are latitude and longitude

EG orogen. The Ghost Crab deposit, spatially associated with the Mt Marion albite-spodumene pegmatites (78 Mt at 1.37% Li_2O; Smith and Ross 2017), represents a new skarn-related style, because sodic anthophyllite-cummingtonite-albite contact zones in paragneiss constitute gold ore. At Chalice in the Pioneer Dome Li-Cs pegmatite district, syn-gold granitic intrusions are albitized and altered to auriferous endoskarn.

The classification of the Archean high-T (650–450 °C) deposits as intrusion-related skarns (Mueller 1991, 1992, 1997a) is controversial. In reviews (Meinert et al. 2005), "Au skarns in regional metamorphic terranes" are treated as a group transitional to "orogenic" deposits. In the orogenic model, "skarn-like" deposits form at convergent plate margins from non-magmatic H_2O-CO_2 fluids infiltrating regional shear zones. They are classified as "hypozonal" amphibolite-facies deposits (Groves et al. 1998; Goldfarb et al. 2005; Goldfarb and Pitcairn 2023). In the Discussion, we evaluate the orogenic model in relation to granite-pegmatite associated gold skarn deposits in the Yilgarn Craton, and to representative deposits in other Archean cratons. The combined evidence indicates that the high-PT Archean deposits represent a new Au-Ag class of intrusion-related reduced ore skarns complementary to the other classes of skarn deposits (Fe, Cu, Zn-Pb, W, Mo, Sn) reviewed in Einaudi et al. (1981).

Field work and methods

Explanatory notes on gold production, and reviews of skarn terminology, subcalcic amphiboles and cordierite in skarn systems, LCT pegmatites, and the mineral abbreviations used (Whitney and Evans 2010) are part of the Electronic Supplementary Material (ESM), the main data repository in this study. The Copperhead, Chalice, and Ghost Crab gold skarn deposits, closed more than 20 years ago, were studied in 1995–1997 during consulting work. In the ESM, the field work carried out at each deposit, and the analytical methods used are described in detail. They include the petrographic examination of thin and polished sections in transmitted and reflected light, and the mineralogical and geochemical analysis of whole-rock samples by X-ray diffraction (XRD) and X-ray fluorescence (XRF), respectively.

ESM Table 1 provides an overview of the radiometric ages (±2-sigma) of LCT pegmatites and late- to post-orogenic granites in the central and eastern Yilgarn Craton. ESM Table 2 lists the ages of orthogneiss batholiths and sills, late- to post-orogenic granite-pegmatite and norite intrusions, and of aureole metamorphism in the 3.0 Ga Southern Cross greenstone belt. The U-Pb ages quoted are based on the decay constants in Steiger and Jäger (1977). The Rb-Sr ages were recalculated using the revised ^{87}Rb decay constant in Villa et al. (2015), whereas the Ar-Ar ages are cited as published.

ESM Table 3 contains the $^{207}Pb/^{206}Pb$ ages of zircon xenocrysts in the youngest granite suite, and ESM Table 4 the published analyses of indicator minerals in fractionated pegmatites. ESM Table 5 summarizes the setting, mineralogy and geochronology of gold skarn deposits (10–63 t Au) and associated granitic intrusions in the 3.0 Ga Southern Cross greenstone belt, and of gold skarn and skarn-quartz vein deposits in the 2.7 Ga Kalgoorlie Terrane. The energy-dispersive EPMA data of skarn minerals from Nevoria, the type locality of an intrusion-related Archean gold deposit (Meinert et al. 2005; Sciuba et al. 2020) are compiled in ESM Table 6, and the wave-length dispersive EPMA data of assemblages with subcalcic amphiboles in ESM Table 7.

Regional geologic setting

The Western Gneiss and the central Youanmi terranes in the Yilgarn Craton constitute the foreland of the Eastern Goldfields (EG) fold belt, a 2.7–2.6 Ga continental-margin orogen composed of at least three stratigraphically distinct internal terranes (Cassidy et al. 2006). In the eastern part of the foreland (Fig. 1), quartzites marked by detrital zircons up to 4.4 Ga old (Thern and Nelson 2012) underlie the main 3.0 Ga komatiite-basalt supracrustal succession correlated regionally by a marker horizon of banded iron formation. Minor ca. 2.98–2.95, 2.82–2.80, and 2.73 Ga old volcano-sedimentary belts are preserved in local synforms (Watkins and Hickman 1990; Chen et al. 2003). The Kalgoorlie Terrane in the EG orogen (Fig. 1) is distinguished by its 2.73–2.65 Ga greenstone-greywacke-conglomerate succession deposited in a rift west of its coeval andesite-dacite volcanic arc (Barley et al. 2008; Mueller et al. 2020).

More than 75 per cent of the erosion surface of the Yilgarn Craton are underlain by mid-crustal granite batholiths. In the Youanmi Terrane bordering the EG orogen (Fig. 1), the batholiths are composed of at least four generations of granitoids, the older ones recrystallized to granofels or orthogneiss. The main periods of emplacement are dated at ca. 2.94–2.91 Ga, 2.83–2.80 Ga, 2.78–2.69 Ga, and 2.67–2.62 Ga (ESM Tables 1 and 2). Plutons of the three older generations are mainly composed of granodiorite and granite but include quartz diorite and trondhjemite-tonalite (Bettenay 1977; Watkins and Hickman 1990).

The youngest "post-kinematic" generation consists of peraluminous I-type biotite granites, lesser granodiorites, and granitic pegmatites (Table 1). They are subdivided into late-orogenic (2675−2655 Ma) and post-orogenic (2655−2620 Ma) based on the timing of the youngest folding phase (2655 Ma) in the Kalgoorlie Terrane of the EG orogen (Mueller et al. 2020). The Wave Rock and Lake Johnston batholiths (Fig. 1) represent large composite intrusions in the southeast Youanmi Terrane. In the Lake Johnston batholith, 40% of the U-Pb zircon emplacement ages ($n=15$) are late-orogenic and 60% post-orogenic (ESM Table 1). The $^{207}Pb/^{206}Pb$ ages of zircon xenocrysts indicate melt interaction with orthogneiss and with the lower continental crust (3.4–3.7 Ga). They also suggest a wider range of emplacement ages (2.96–2.90 Ga, 2.86–2.80 Ga) for the two oldest granitoid generations (ESM Table 3).

Half the cassiterite (42,399 t at 70% SnO_2) and tantalite-columbite concentrates (6,155 t at 28–42% Ta_2O_5; Witt 1992) in Western Australia were produced from the giant Greenbushes pegmatite at the southwestern margin of the Yilgarn Craton (inset in Fig. 1), also mined for spodumene since 1985. Resources still amount to 157 Mt at 2.25% Li_2O (Partington 2017). The Greenbushes pegmatite (2527±2 Ma; Partington et al. 1995) is zoned, displays extremely fractionated Rb/Sr ratios, and is strongly peraluminous (Table 1). Calcite, Ca-scapolite, epidote, biotite, anthophyllite, holmquistite, tourmaline, and arsenopyrite in the ultramafic-mafic volcanic host rocks (Partington 1990; Partington et al. 1995) indicate metasomatism caused by a magmatic fluid containing CO_2, Ca, K, Li, B, and As.

Southern Cross greenstone belt

To the west, the Southern Cross greenstone belt (SCB) is in contact with a magmatic arc of late- to post-orogenic, equigranular to seriate biotite granites enclosing porphyritic or K-feldspar megacrystic plutons (Fig. 2). Most are classified as monzogranite by normative mineralogy (Mueller et al. 2004), and are weakly peraluminous (<1.1) and magnetite-bearing (mag > ilm) permitting the classification as I-type magnetite-series (Table 1). The megacrystic Wave Rock granite, dated at 2631±3 Ma (ESM Table 2), has a Rb/Sr ratio of 1.32 and belongs to the least evolved "biotite granite" facies of the fertile rare-metal suite in Cerný and Meintzer (1988). The plutonic arc encloses enclaves of orthogneiss, and rafts of amphibolite- to granulite-facies greenstone. Enclaves bordering the Wave Rock and Karalee batholiths contain hydrothermal magnetite-pyrite mineralization (Fig. 2) estimated at 50–100 million metric tonnes (Mt) at Hyden and Mt Vernon (13–14% Fe; see ESM).

On its eastern side, the SCB is mostly bounded by orthogneiss dated by an average Rb-Sr total-rock age of 2706±65 Ma. The Ghooli Dome batholith (GDB; Fig. 2) is composed of granitic gneisses, which record U-Pb zircon ages of 2775±10

Table 1 Classification of post-orogenic granite-pegmatite intrusions (2.65–2.53 Ga), Youanmi and Kalgoorlie terranes, east-central Yilgarn Craton, and the Greenbushes LCT pegmatite in the southwest Gneiss Terrane, Western Australia

Post-orogenic intrusion (<2655 Ma)	Fractionation		CIPW corundum	Al_2O_3 / (K_2O+ Na_2O+CaO)	K / (K+Na)	Total FeO	Fe_2O_3 / FeO	Indicator minerals	Associated ore deposit
	SiO_2 (wt%)	Rb/Sr	(wt%)	molar	atomic	(wt%)		(vol%)	
Bridgetown-Greenbushes LCT pegmatite district, southwest Gneiss Terrane									
Logue Brook Kfs granite	74.20	2.33	1.41	1.10	0.52	1.81	0.73		
Greenbushes North pegm.	66.64	21.09	3.96	1.12	0.06	1.74	n.d.	Spd, cst, tan	LCT pegmatite
Greenbushes Main pegm.	70.14	77.65	4.30	1.29	0.30	1.14	n.d.	Spd, cst, tan	LCT pegmatite
Southern Cross gold and LCT pegmatite district, southeast Youanmi Terrane									
Nevoria Zone A pegmatite	75.45	29.00	2.44	1.20	0.39	0.66	n.d.	Grt, rt	Au skarn
Nevoria Zone B peg-gran.	74.84	25.73	1.74	1.13	0.43	0.57	n.d.	Rt, sil	Au skarn
Nevoria Zone C granite	75.94	12.43	0.42	1.03	0.50	0.82	0.29	0.1 mag, ilm	Au skarn
Copperhead-Radio granite	71.60	8.06	1.83	1.13	0.59	0.68	n.d.	Grt	Au vein, skarn
Edna May pegm. granite	74.56	5.63	0.23	1.01	0.44	1.49	n.d.	0.5 mag, aln	Au skarn
Lake Seabrook granite	74.37	1.37	0.42	1.02	0.42	1.14	0.83	0.3 mag, aln	W skarn
Mt Correll granite	73.59	2.90	0.39	1.01	0.48	2.06	0.79	0.5 mag, ttn	ath-crd, skarn
Mt Correll south, granite	72.01	0.48	0.00	0.98	0.39	2.06	1.14		
Mt Correll south, granite	72.27	0.63	0.40	1.01	0.37	1.70	0.21		
Mt Correll south, granite	72.96	0.86	0.82	1.04	0.38	1.36	1.79		
Wave Rock Kfs granite	71.01	1.32	0.30	1.01	0.45	2.49	0.54	1 mag, ttn,	Magnetite
Wave Rock granite	73.87	0.63	0.67	1.05	0.44	1.03	0.80	0.1 ilm, py,	Magnetite
Wave Rock granite	72.62	1.56	0.90	1.06	0.49	1.66	1.16	ccp	
Murchison gold and LCT pegmatite district, northwest Youanmi Terrane									
Big Bell porphyritic granite	72.49	3.98	1.13	1.07	0.40	1.64	n.d.	Ttn	Au
Koolanooka granite	76.62	5.43	0.77	1.06	0.49	1.84	0.49		
Damperwah granite	71.95	1.02	0.81	1.05	0.48	3.55	0.14		
Damperwah granite	70.63	0.67	0.49	1.00	0.44	4.58	0.31		
Pioneer-Norseman gold and LCT pegmatite district, southwest Kalgoorlie Terrane									
Chalice, granite Dike-2	73.53	1.87	0.32	1.01	0.49	1.35	n.d.	0.5 mag, rt	Au skarn
Chalice, granite Dike-3	74.46	2.51	0.29	1.01	0.45	1.00	n.d.	0.5 chl-mag	Au skarn
Chalice, main granite	75.31	1.89	1.02	1.08	0.38	1.34	1.12	0.3 mag, py	Au skarn
Chalice, main granite	72.96	0.45	0.70	1.04	0.25	1.27	n.d.	Py	Au skarn
Norseman, dike average	77.92	3.58	1.23	1.10	0.38	0.95	n.d.	Grt	Au vein, skarn
Norseman, Crown dike	76.57	3.44	0.12	1.01	0.34	0.78	0.18	Py	Au vein, skarn
Norseman, Dundas granite	75.96	8.48	0.83	1.06	0.52	1.06	0.71		Au vein, skarn
Classification criteria as I-type and/or magnetite-series									
I-type classification	Fractionation		<1.0	<1.1	<0.5				
Magnetite series	Fractionation						>0.5	>0.2% mag	

Geochemical data: Bettenay (1977); Blight et al. (1981); Spray (1986); Watkins and Hickman (1990); Perring et al. (1990); Dalstra (1995); Partington et al. (1995); Qiu (1997); Mueller 1997c); Bucci et al. (2002); Mueller et al. (2004). n.d. not determined

U-Pb zircon ages: Wiedenbeck and Watkins (1993), Partington et al. (1995), Mueller et al. (1996), Nemchin and Pidgeon (1997), Qiu and McNaughton (1999), Qiu et al. (1999), Mueller et al. (2004), Bucci et al. (2004)

Granite classification: I-type in Chappell and White (2001), magnetite series in Ishihara (1981) and Takagi and Tsukimura (1997)

to 2691 ± 7 Ma but enclose enclaves 2.93–2.91 Ga old. Granite and granodiorite sills in the greenstone belt were emplaced at 2.93–2.81 Ga setting a minimum of 2934 ± 7 Ma for the SCB komatiite-basalt succession, and for the conformable upper greywacke-gabbro sill succession, which records a zircon depositional age of 2983 ± 8 Ma (ESM Table 2). The banded iron formation marker horizon outlines tight to isoclinal regional folds refolded during the emplacement of the Ghooli Dome and other batholiths (Mueller et al. 2004).

The greenstones are metamorphosed to amphibolite facies in aureoles contouring the orthogneiss-granite-greenstone contact (Ahmat 1986). In the km-wide aureole of the Ghooli Dome, where many gold skarns are located (Fig. 2), metamorphic assemblages and steeply plunging mineral lineations in

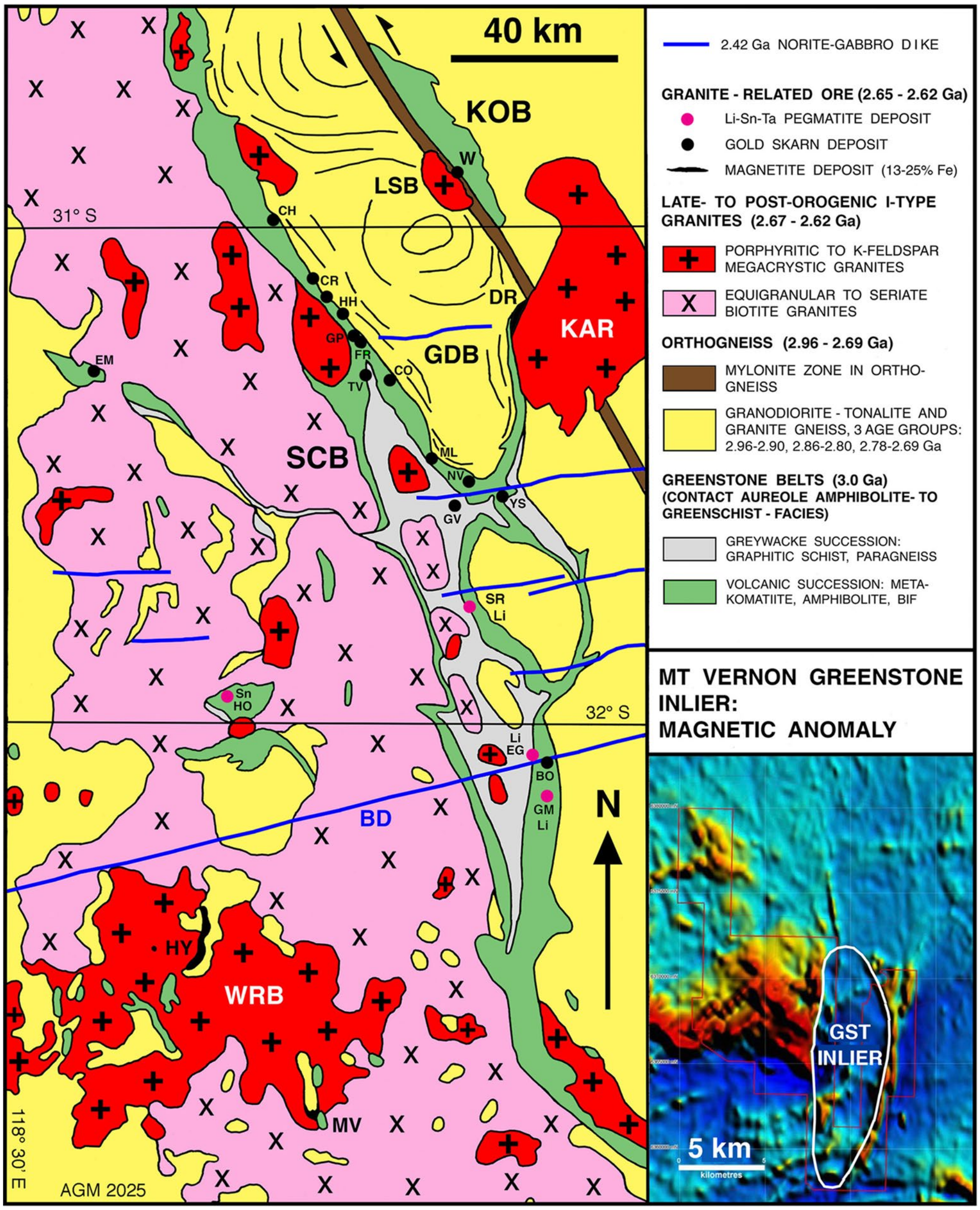

Fig. 2 Geologic map of the Southern Cross area (modified from Gee 1982; Chin and Smith 1983; Chin et al. 1984) showing the 3.0 Ga Southern Cross (SCB) and Koolyanobbing (KOB) greenstone belts, the Ghooli Dome batholith (GDB), the western plutonic arc formed by late- to post-orogenic granites, and the Binneringie norite dike (BD). Magnetite-pyrite mineralization at Hyden (HY), Mt Vernon (MV; inset map) and Duladgin Rock (DR) is associated with the Wave Rock (WRB) and Karalee (KAR) granites (Magnetic Resources 2010). Gold skarn deposits (10–63 t Au; ESM Table 5): Bounty (BO), Copperhead (CH), Corinthian-Hopes Hill (CR-HH), Cornishman (CO), Edna May (EM), Fraser's (FR), Golden Pig (GP), Great Victoria (GV), Marvel Loch (ML), Nevoria (NV), Transvaal (TV), Yilgarn Star (YS). Tungsten skarn (W) at Lake Seabrook (LSB). LCT pegmatites: Earl Grey (EG), Gem (GM), Holleton (HO), Split Rocks (SR)

greenstone indicate crystallization at a lithostatic pressure of 400 MPa during batholith emplacement at about 15 km depth (Dalstra et al. 1998). At the Copperhead mine, zircons in altered quartz porphyry sills record two concordant U-Pb ages: 2912±5 Ma and 2772±5 Ma (ESM Table 2). The younger one is within error of the granite age in the adjacent batholith, and interpreted to date Ghooli Dome aureole metamorphism due to the recrystallization of metamict zircons in the 2.91 Ga sills (Mueller and McNaughton 2000). At the western margin of the SCB, a monazite-in-andalusite age of 2671±14 Ma in graphitic paragneiss indicates diachronous aureole metamorphism. Regional Ar-Ar muscovite and Rb-Sr biotite ages of 2.61–2.59 Ga record mica closure to Ar and Sr diffusion at 300–350 °C during terrane cooling (ESM Tables 1 and 2).

The northeastern orthogneiss in the Ghooli Dome is transected by mylonites of the Koolyanobbing shear zone, mirrored by proto-mylonites in the less deformed border gneiss at the southwestern margin. Shallowly plunging mineral lineations and porphyroclasts indicate sinistral transcurrent movement (Libby et al. 1991; Bloem et al. 1994). The Koolyanobbing mylonites are crosscut by the post-tectonic Lake Seabrook granite dated at 2656 ± 3 Ma (Fig. 2; ESM Table 2). The shear zone, though crustal-scale, does not contain gold deposits.

Granite-pegmatite associated mineralization

Apart from disseminated magnetite-pyrite mineralization, three other styles are spatially associated with late- to post-orogenic granite-pegmatite complexes in the east-central Yilgarn Craton: (1) subeconomic tungsten skarn; (2) gold skarns, skarn-quartz vein, and quartz vein deposits, and (3) LCT pegmatites.

Lake Seabrook tungsten skarn

At Lake Seabrook, weakly fractionated biotite-muscovite granite (Rb/Sr = 1.37; Table 1) and associated garnet-fluorite-bearing pegmatite dikes cut across orthogneiss and mylonites close to the contact with the Koolyanobbing greenstone belt (Fig. 2). At the orthogneiss-greenstone contact, a 20–50 m wide and more than 6 km long zone of scheelite-bearing quartz-veined skarn occurs in the greenstones about 1 km northeast of the exposed massive granite. In this zone, hornblende-actinolite-biotite, diopside-clinozoisite and actinolite-epidote-quartz skarns and talc-chlorite schist replace foliated meta-komatiite and amphibolite. Drill-core intersections indicate high tungsten grades (0.1–0.5 wt% WO_3), and anomalous molybdenum (100 ppm) and bismuth (25 ppm). An economic resource has not been defined.

Gold skarn and skarn-quartz vein deposits

Most of the post-orogenic granite-pegmatite intrusions associated with gold skarns are characterized by higher Rb/Sr ratios (3–29) than the Wave Rock and Lake Seabrook plutons, and are considerably more fractionated (Table 1). Garnet-muscovite granite north of the Copperhead deposit (Dalstra et al. 1998) and layers of such granite in the roof zone of the Nevoria intrusion correspond to the "fine-grained leucogranite", whereas the pegmatite-rich Nevoria two-mica granite corresponds to the "pegmatitic leucogranite" of Cerný and Meintzer (1988), evolved facies intermediate in rare-metal fertility. Both intrusions and the granitic dikes at Norseman are corundum normative (1.23–2.44) and have molar Al_2O_3/(K_2O + Na_2O + CaO) > 1.1 ratios. Skarn-associated pegmatites contain accessory almandine (23–31 mol% spessartine; ESM Table 4), blue manganoan apatite, black tourmaline, and rare magnetite, Mg-Fe-Zn spinel, molybdenite and corundum.

The characteristic features of granite-pegmatite-related gold skarn deposits in the Southern Cross Belt, and of skarn and skarn-quartz vein deposits in the south Kalgoorlie Terrane are summarized in ESM Table 5. Gold mineralization has been dated at 2640 − 2620 Ma in five deposits, and in four the mineralization age agrees within error with the emplacement age of the associated post-orogenic intrusions (Fig. 3). In addition, the southern pegmatite dike at Marvel Loch breaks up in the foliated skarn zone into albite-garnet-chlorite pods with inclusions of native gold suggesting syn-mineralization emplacement (Mueller 1991). The Nevoria and three of the largest (> 31 t Au) gold skarns (Marvel Loch, Edna May, Yilgarn Star) terminate 250–800 m down plunge at thick granite-pegmatite complexes, whereas ore bodies at Bounty and Copperhead were mined more than 900 m down plunge without disruption by felsic intrusions. Mineral assemblages constrain the PT-conditions during skarn formation at Marvel Loch to 400 ± 100 MPa and 640–500 °C (Mueller et al. 1991a, b), at Edna May to 400 ± 200 MPa and 650–600 °C (Hagemann and Cassidy 1999), and at Corinthian-Hopes Hill to 300–400 MPa and 540–450 °C (Bloem et al. 1994). Temperatures during the retrograde stage fell to < 400 °C as indicated by the common occurrence of prehnite (e.g., Nevoria; ESM Table 6).

In the SCB, the gold skarn deposits (Au: Ag = 1:1 to 3:1) are controlled by sheared lithologic contacts of moderate displacement (<200 m). Late-stage skarn is post-kinematic (Mueller 1991, 1997a, b, c). Many gold skarns and associated intrusions are offset at brittle-ductile faults, a dextral set striking NNE to NE and a younger sinistral one striking E to ENE. Most faults are barren but a few in the northern SCB contain Au ± Mo quartz veins (<2.6 t Au) bordered by biotite-chlorite alteration.

The skarn-quartz vein deposits (Au: Ag = 1:5) at Norseman in the southern Kalgoorlie Terrane are associated with garnet-bearing porphyry dikes (Table 1) marked by chondrite-normalized REE-patterns with negative Eu anomalies and affinities to Sn-U enriched granites (Perring et al. 1990). The deposits and dikes, some probably albitized (ESM Table 5), are spread across a zoned district (Thomas et al. 1990). In the center, early skarn (0.5 g/t Au) replaces amphibolite and ultramafic amphibole-chlorite rock in reverse shear zones, and consists of hornblende + biotite + calcic plagioclase + pyrrhotite and quartz-calcite-actinolite veins formed at about 480 °C and 300 MPa pressure (Mueller 1992). At the district margin, the early skarn lacks amphibole, formed at 450 °C, contains auriferous arsenopyrite, and grades outward into wide chlorite-calcite ± pyrrhotite alteration. Most of the gold is in post-skarn quartz veins with chlorite-sericite partings, which averaged 10.6 g/t Au, 51.6 g/t Ag, 500 g/t Pb and 190 g/t W in 1983–1985 (Mueller 1992). Across the district, the quartz-rich ore is zoned from inner high Ag/Au and low As/Au to outer low Ag/Au and high As/Au ratios (Thomas et al. 1990).

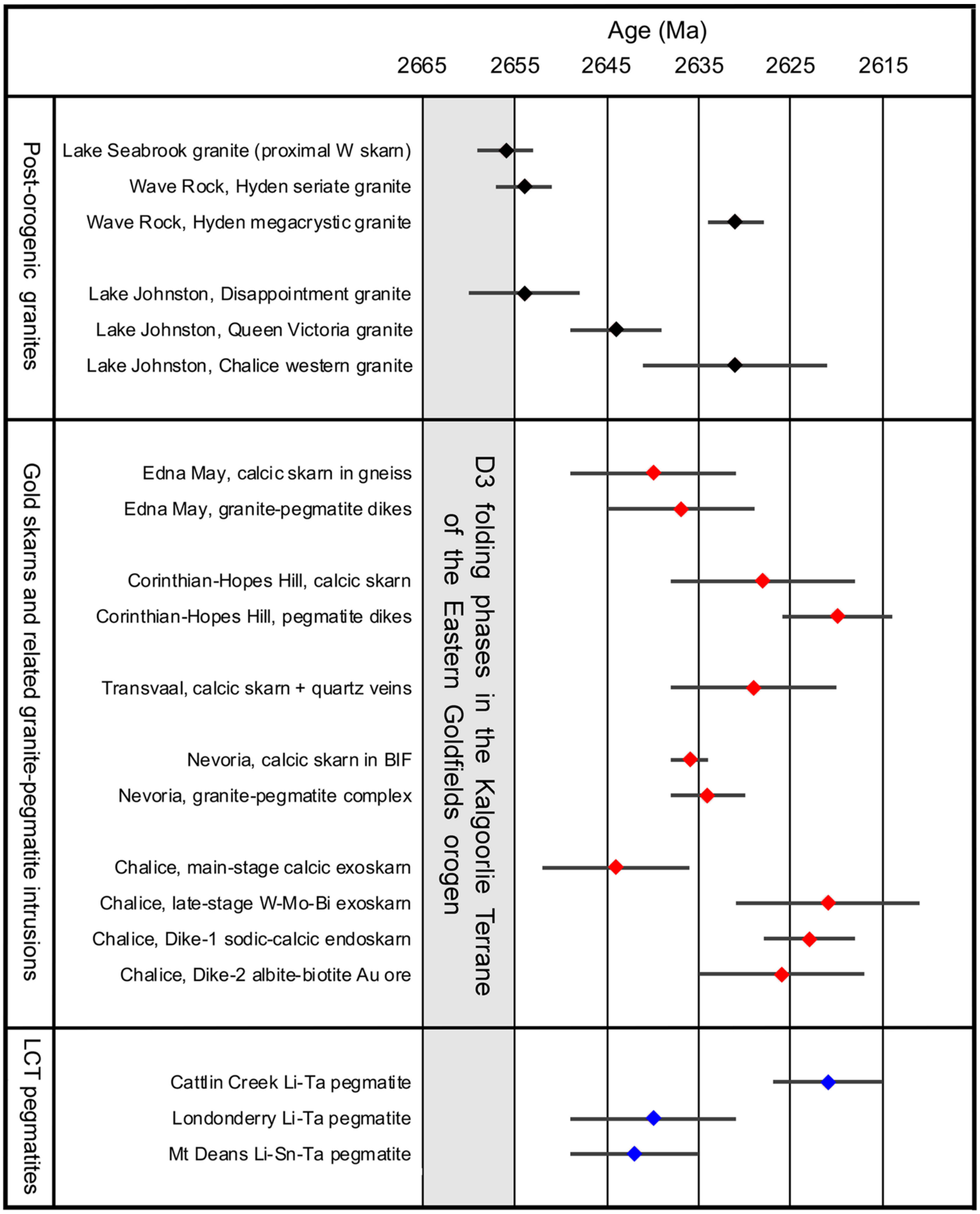

Fig. 3 Diagram showing the radiometric ages (±2-sigma error) of post-orogenic I-type granites, of gold skarn deposits and spatially associated granite-pegmatite intrusions, and of LCT pegmatites in the east-central Yilgarn Craton, Western Australia. The youngest folding phases (D3) in the Kalgoorlie Terrane (Mueller et al. 2020) define the marker period for the term "post-orogenic". Data, analytical details, and references are in ESM Tables 1, 2 and 5

Rare-metal pegmatites

In the east-central Yilgarn Craton, spodumene is mined from the Cattlin Creek pegmatite (16.7 Mt at 1.28% Li_2O and 159 g/t Ta_2O_5) and from the Mt Marion pegmatite field (78 Mt at 1.37% Li_2O), while the Split Rocks (11.9 Mt at 0.72% Li_2O), Earl Grey (189 Mt at 1.5% Li_2O), and Londonderry spodumene pegmatites are explored or prepared for production (Sweetapple et al. 2019; Phelps-Barber et al. 2022; Zenith Minerals 2024; Future Battery Minerals 2025). The lepidolite Rb-Sr model ages of pegmatites in the northwest Youanmi Terrane suggest a relationship to late-orogenic granites, whereas the Ta-Nb oxide U-Pb ages of pegmatites in the southeastern Youanmi and Kalgoorlie terranes constrain pegmatite emplacement to the post-orogenic period (ESM Table 1), coeval with the formation of gold skarn deposits (Fig. 3). Skarn-related and LCT pegmatites also share accessory minerals including Fe-Mn garnet, apatite, tourmaline, magnetite, and gahnite-hercynite spinel (Witt 1992; Smith and Ross 2017).

The Cattlin Creek, Earl Grey, and Mt Marion pegmatites belong to the albite-spodumene subtype, and require a pressure of 300–400 MPa to stabilize the assemblage spodumene + quartz (London 1984). They are essentially unzoned. The Cattlin Creek pegmatite consists of spodumene megacrysts oriented sub-perpendicular to the intrusive contacts, which are set in a medium-grained quartz-albite ± muscovite groundmass with aplite layers. In the eastern part, the pegmatite sheet contains lepidolite-rich units marked by quartz pods, cavities, and accessory tourmaline and fluorite (Sweetapple et al. 2019). The branching Earl Grey pegmatite, too, lacks internal zoning, and consists of quartz-albite-microcline assemblages with minor biotite, muscovite and tourmaline. Spodumene is predominant in the thick central part but progressively altered to petalite at the western, and to petalite or cookeite (Li-chlorite) at the eastern margin. The pegmatite margins are offset at faults parallel to the north-striking greenstone-greywacke contact (SQM, Sociedad Quimica y Minera de Chile 2022). The Earl Grey pegmatite is located 1 km WNW of the Bounty gold skarn deposit (Fig. 2), and dips at shallow angles north below open pits mined for gold (Fig. 4a).

The Mt Marion pegmatites also have local border zones of spodumene megacrysts but consist largely of randomly oriented spodumene 2–5 mm long (10–45 vol%), interstitial quartz (15–45%), albite-oligoclase (5–43%), microcline (2–25%), and muscovite (3–7%; Smith and Ross 2017). The main host rocks are amphibolites composed of Mg-hornblende and oligoclase. Close to the intrusive contact, the amphibolites contain Li-enriched hornblende (ESM Table 4), disseminated holmquistite and/or tourmaline indicating Li-B metasomatism (Wilkins et al. 1970).

The Nevoria and Copperhead gold skarns

The principal features of the source-proximal Nevoria and the distal Copperhead gold skarn systems in the Southern Cross greenstone belt are summarized for comparison with those in the Mt Marion-Wattle Dam and Pioneer Dome Au-Li districts at the western margin of the Kalgoorlie Terrane.

Nevoria gold skarn system

The Nevoria system is illustrated in a cross section through the calcic-potassic alteration zone, and through the pegmatite roof of the pluton below (Fig. 4b). Skarn bound to lithologic contacts in the 3.0 Ga greenstone succession is centered on beds of grunerite-quartz ± magnetite banded iron formation (BIF 1 to 3) and minor almandine-bearing quartz-biotite-graphite schist. The BIF beds mark the transition from tholeiitic amphibolites in the footwall to ultramafic amphibole-chlorite rocks (meta-komatiites, > 18 wt% MgO anhydrous) in the hanging wall. In amphibolite, the plagioclase composition decreases from andesine (An30-50) in the north to oligoclase (An15-30) in the south away from the contact of the Gooli Dome batholith. Peak metamorphic temperature is estimated at 610 ± 50 °C based on hornblende-plagioclase and almandine-biotite exchange thermometry (Mueller et al. 2004). The skarns vary from reduced (about 90% by volume) to moderately oxidized according to mineralogy (ESM Table 6).

Reduced skarns Reduced ore skarn (6–7 g/t Au, 2–3 g/t Ag) is confined to the BIF beds, which are partly replaced by calcic hedenbergite-actinolite and almandine-hornblende ± quartz skarns. Both contain 5–15% disseminated pyrrhotite, minor loellingite-arsenopyrite, blue-fluorescent scheelite, rare bismuth tellurides, and maldonite. Native gold is enclosed in and intergrown with hedenbergite, almandine, quartz, and pyrrhotite. The zoned almandine-hornblende bands and veins are characterized by biotite, cummingtonite, tourmaline, zircon, Ti-magnetite, and ilmenite inclusions in almandine, and by allanite inclusions in both almandine and hornblende. Mixed prograde ore skarn is enriched in TiO_2, Al_2O_3, CaO, K_2O, CO_2, sulfur, Au, Ag, Bi, Cu, Ba, Cs, Li, Rb, Sr, Y, Nb, Th, W and Zr relative to least-altered BIF, a particularly pure precursor rock (Mueller 1997a). Chlorite and stilpnomelane are retrograde.

In contact skarns replacing amphibolite (< 0.5 g/t Au), the local enrichment of calcium relative to potassium varies. Most skarns are composed of replacement bands zoned at the cm-scale from core to margin: diopside → hornblende-pargasite → biotite → chlorite, and calcite + microcline → plagioclase → zoisite + muscovite. These bands are intercalated with 5–50 cm thick, massive almandine-bearing skarn composed of: (1) almandine porphyroblasts (1–5 vol%), biotite, cummingtonite, and accesssory anthophyllite and ilmenite set in a felsic groundmass of quartz + plagioclase (An50-97); and (2) almandine (5–20%) set in a mafic groundmass of biotite-chlorite, minor hornblende-pargasite, cordierite + gedrite, and accessory tourmaline and Ti-magnetite. Retrograde prehnite and zoisite + muscovite after plagioclase are widespread.

Oxidized skarns Magnesian skarns characterized by the assemblage calcite-magnetite-diopside are stratabound to the contacts of meta-komatiite (Fig. 4b), and form cross-cutting zoned veins in amphibolite and BIF. In veins, the inner calcite-magnetite zone contains variable amounts of Mg-rich chlorite (up to 20 vol%), humite group minerals, phlogopite or stilpnomelane, and retrograde serpentine. The outer zone consists of diopside, actinolite, and hornblende.

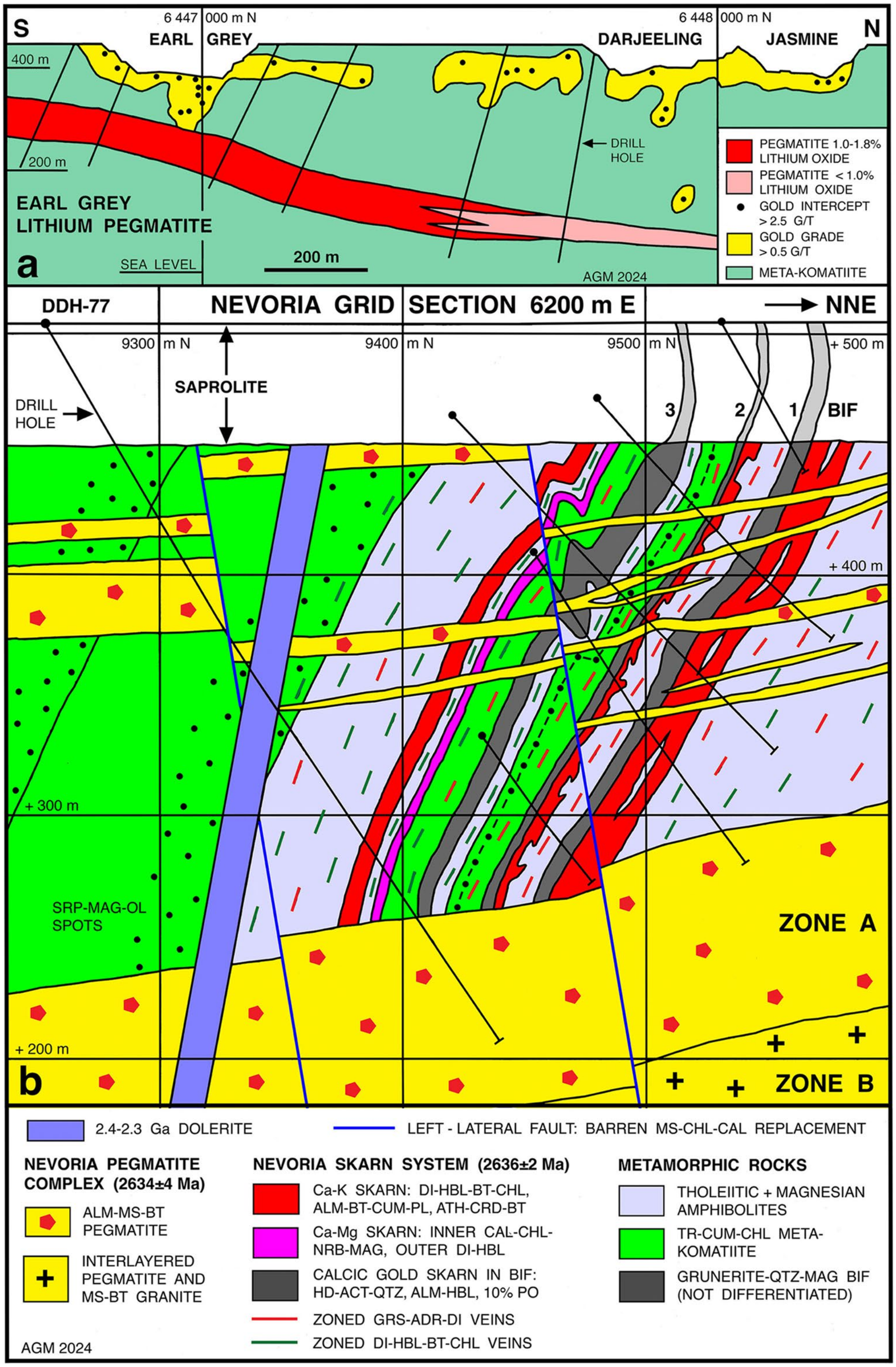

Fig. 4 Sections illustrating the spatial relationship between fractionated granitic pegmatites and gold skarn deposits. **(a)** Longitudinal projection showing the Earl Grey spodumene pegmatite below the Twinings Group of open pits mined for gold, coordinates are Map Grid Australia (modified from Kidman Resources 2017). **(b)** NNE-SSW cross section at 6200 m mine grid east through the alteration zone of the Nevoria gold skarn deposit and the coeval pegmatite-granite complex below (Mueller et al. 2004), based on the lithologic log of drill core DDH-77, and mapping on the main shaft 3 level and in the open pits (Mueller 1997a)

Some magnesian skarns are mineralized with disseminated (2–5 vol%) pyrite, pyrrhotite, rare gersdorffite, and niccolite.

Zoned calcic grossular-diopside veins 3–10 cm thick are widespread in amphibolite and meta-komatiite but absent in BIF (Mueller 1997a). They are moderately oxidized as the gossular contains up to 37 mol% andradite. The grossular is in contact with yellow-fluorescent scheelite (1.1–1.5 wt% Mo; Sciuba et al. 2020), and with interstitial calcite, quartz, microcline, and plagioclase (An 04–16). The inner assemblage is partly replaced by retrograde clinozoisite-epidote and prehnite. The outer diopside zones are bordered by thin rims of hornblende or grade into halos of disseminated hornblende.

Outer alteration Outer alteration comprises zoned diopside-hornblende and hornblende-biotite ± chlorite bands (Fig. 4b). Disseminated olivine porphyroblasts occur in broad zones within the southern ultramafic volcanic succession, perhaps bound to the basal parts of meta-komatiite flows. Most porphyroblasts are retrograded to serpentine + magnetite, an assemblage imparting a magnetic signature to the Nevoria hydrothermal system.

PTX of skarn formation Estimates based on the Fe-Mg exchange thermometry of almandine-biotite and almandine-hornblende pairs in ore skarn vary from 520 ± 75 °C to 632 ± 50 °C. Ferro-hornblende and -actinolite in reduced hedenbergite-bearing skarn have $Mg/(Mg+Fe^{2+})$ ratios of 0.23–0.43 (ESM Table 6). The Fe-endmember of actinolite has an upper thermal stability limit of 560 °C at 350 MPa, the lowest amongst the calcic amphiboles (Ernst 1968), compatible with a temperature window of 550–650 °C for prograde skarn formation. Garnet-biotite-cummingtonite-anorthite assemblages in amphibolite-hosted skarn constrain the pressure to 300–400 MPa. This pressure converts to 11–15 km depth at lithostatic load. The stability of retrograde prehnite suggests that the fluid cooled to less than 400 °C, probably to the ambient temperature at mid-crustal depth (± 350 °C; Mueller et al. 2004).

Fluid inclusions in grossular and diopside from zoned veins and in quartz from hedenbergite-actinolite gold skarn homogenized to liquid at T_h = 190–380 °C (Fan et al. 2000). The P-T estimates above require a correction of > 200 °C to trapping temperatures. The fluid salinities calculated (0.1–10 wt% $NaCl_{eq}$) are approximate because first-melting temperatures indicate the presence of $CaCl_2$ and $MgCl_2$. Aqueous-carbonic inclusions (X_{H2O} = 0.46–0.90) in oxidized grossular-diopside veins always contained more carbon dioxide than methane (molar CO_2/CH_4 of carbonic phase = 15–100). In fluids enclosed in reduced gold skarn (X_{H2O} = 0.22–0.93), the carbonic phase varied from pure carbon dioxide to pure methane (CO_2/CH_4 = 0.01–100). These results suggest a link between gold deposition in BIF (30 wt% FeO) and the reduction of an infiltrating H_2O-CO_2 fluid trapped at > 550 °C at near-critical conditions.

Pegmatite-granite pluton The Nevoria gold skarn has been dated by an allanite-in-almandine U-Pb age at 2635.7 ± 1.2 Ma, and the pegmatite-granite pluton below by a concordant zircon U-Pb age at 2634 ± 4 Ma, both > 90 Ma younger than amphibolite-facies metamorphism in the aureole of the Ghooli Dome batholith (Mueller et al. 2004). The pluton is associated with garnet-bearing pegmatite and aplite dikes (Fig. 4b), and zoned from an 80 m thick roof pegmatite (Zone A) to a 95 m thick intermediate zone of interlayered pegmatite and granite (Zone B; 50 vol% each) to fine-grained two-mica granite with pegmatite pods more than 160 m thick (Zone C). The roof Zone A is composed of muscovite-biotite pegmatite, locally segregated into graphic quartz-feldspar and massive quartz, and minor interlayered garnet-muscovite granite characterized by Mn-rich almandine (ESM Table 4). In Zone A, muscovite (5 vol%) is more abundant than biotite (1%) and garnet (0.5–1%). In the deep granite, garnet is absent and iron-rich biotite [Fe/(Fe + Mg) = 0.76] is the only mafic silicate (3–5%) associated with muscovite (0.5–2%) and interstitial sillimanite (0.2%). Quartz-albite myrmekite is common at oligoclase-microcline boundaries. The granite contains rare (0.1–0.2%) magnetite and ilmenite. In Zones A and B, rutile is the only oxide. Whole-rock analyses reveal an increase in CIPW normative corundum from the deep granite (0.42) to the roof pegmatite (2.44), and a concomitant increase in normative albite (Mueller et al. 2004).

Metals like Au, Bi, Cu, Nb and W are enriched in both the Zone A pegmatite and in the gold skarn, whereas other elements are depleted in the pegmatite (Ba, Sr, Th, Zr) but enriched in the skarn (Fig. 5). Like the U-Pb chronology, these enrichment patterns support a genetic link between hydrothermal and intrusive activity. Red dikes of garnet-bearing quartz-feldspar porphyry, marked by internal K-feldspar metasomatism, probably predate the main pegmatite-granite complex suggesting multiple stages of emplacement during skarn formation (Mueller et al. 2004).

Post-skarn faults The Nevoria skarns are displaced by brittle-ductile faults, a dextral set oriented N10-25°E/55–65°E with striations pitching 10–35° south on fault planes, and a sinistral subvertical set striking N75-80°E and offsetting the steeply dipping BIF-beds up to 150 m. Both fault sets control barren, mesothermal muscovite-calcite-chlorite ± biotite alteration in amphibolite. The ENE-faults offset the pegmatite dikes and the zoned pluton, and are younger than 2634 ± 4 Ma. They are crosscut by east-striking dolerite

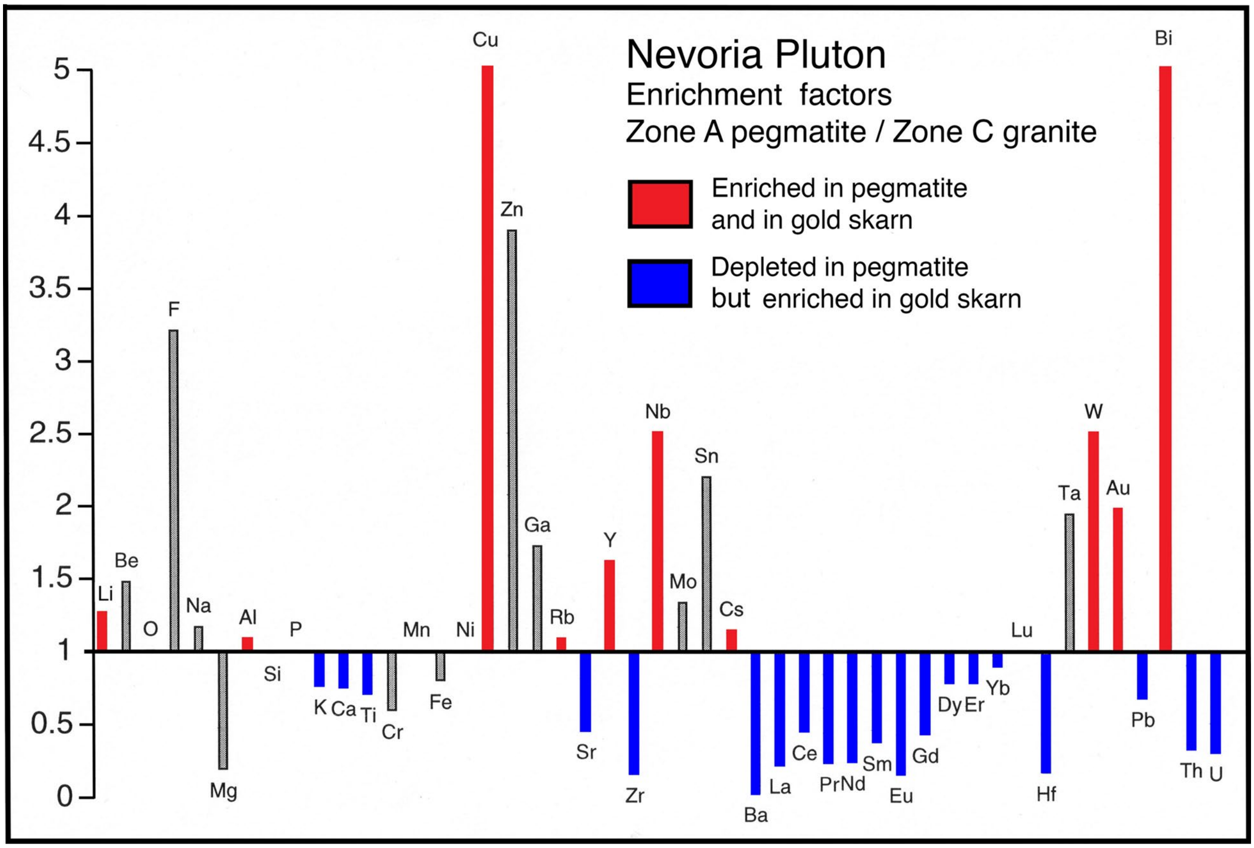

Fig. 5 Element enrichment or depletion in the roof Zone A pegmatite relative to the deep Zone C granite of the Nevoria intrusion (data in Mueller et al. 2004). The colour-coded bars highlight elements enriched in BIF-hosted gold skarn (Mueller 1997a; appendix): red bars indicate elements enriched in both skarn and Zone A, whereas blue bars indicate elements enriched in skarn but depleted in Zone A. The rare earth elements and uranium substitute for Ca in allanite used to date the gold skarn (Mueller et al. 2004), whereas Hf and U substitute for Zr in hydrothermal zircon. These substitutions are evident in the ratio gold skarn (ppm) / least-altered BIF (ppm) for the total REE (8.5), Ce (9), U (18), and Hf (38; this study)

dikes and must be older than 2.3 Ga, the reset muscovite Rb-Sr age in the Zone A pegmatite (ESM Table 2).

Copperhead gold skarn system

The Copperhead Au-Ag skarn deposit in the northern Southern Cross Belt is located 200 m southwest of the Ghooli Dome orthogneiss batholith, and 5–6 km south of a garnet-muscovite granite emplaced into this batholith (Fig. 2). The pluton contains rafts of greenstone and orthogneiss, and outcrops in a 5 × 15 km wide area surrounded by spessartine-bearing pegmatite dikes (Matheson and Miles 1947; Dalstra et al. 1998). The granite is highly fractionated (Rb/Sr = 8.06), enriched in potassium (Table 1), and associated with a 1 km wide zone of metasomatic biotite in the mafic-ultramafic greenstones of the SCB (Keats 1991). The outer pegmatite dikes both predate and postdate quartz-sulfide veins with biotite selvages mined at Radio (2.6 t Au) and Marie's Find (0.39 t Au) in NE-striking faults, and veins mined at Wither's and Rutherford's Find (<0.1 t Au; Keats 1991) in east-striking faults.

At Copperhead, two gold ore bodies termed the Dolomite Lode and the Southern Lode, occur in or adjacent to a bed of quartz-grunerite-magnetite BIF complexly folded into isoclinal synforms plunging 45° NW (Fig. 6). Ore shoots in the Dolomite Lode synform were mined 930 m down plunge to the Main shaft 22 level 680 m below surface. The production from this ore body amounts to 3.4 Mt at recovered grades of 4.22 g/t Au and 1.17 g/t Ag (1952–1966; Chin and Smith 1983). The east-trending Southern Lode synform shortened down-plunge. It closed and became barren below the Main shaft 6 level (Williamson and Barr 1965). Pegmatite and granite dikes are not exposed in the open pit and, apparently, were not encountered underground. The metamorphic host rocks consist of tholeiitic amphibolites northwest of the BIF, and of interbedded high-Mg amphibolites and meta-komatiites to the southeast.

The internally folded ore bodies are enclosed in a broad synform of altered high-Mg amphibolite (0.65% TiO_2). They are bordered by discontinuous lenses of massive hornblende-actinolite-calcite skarn grading into a wide zone

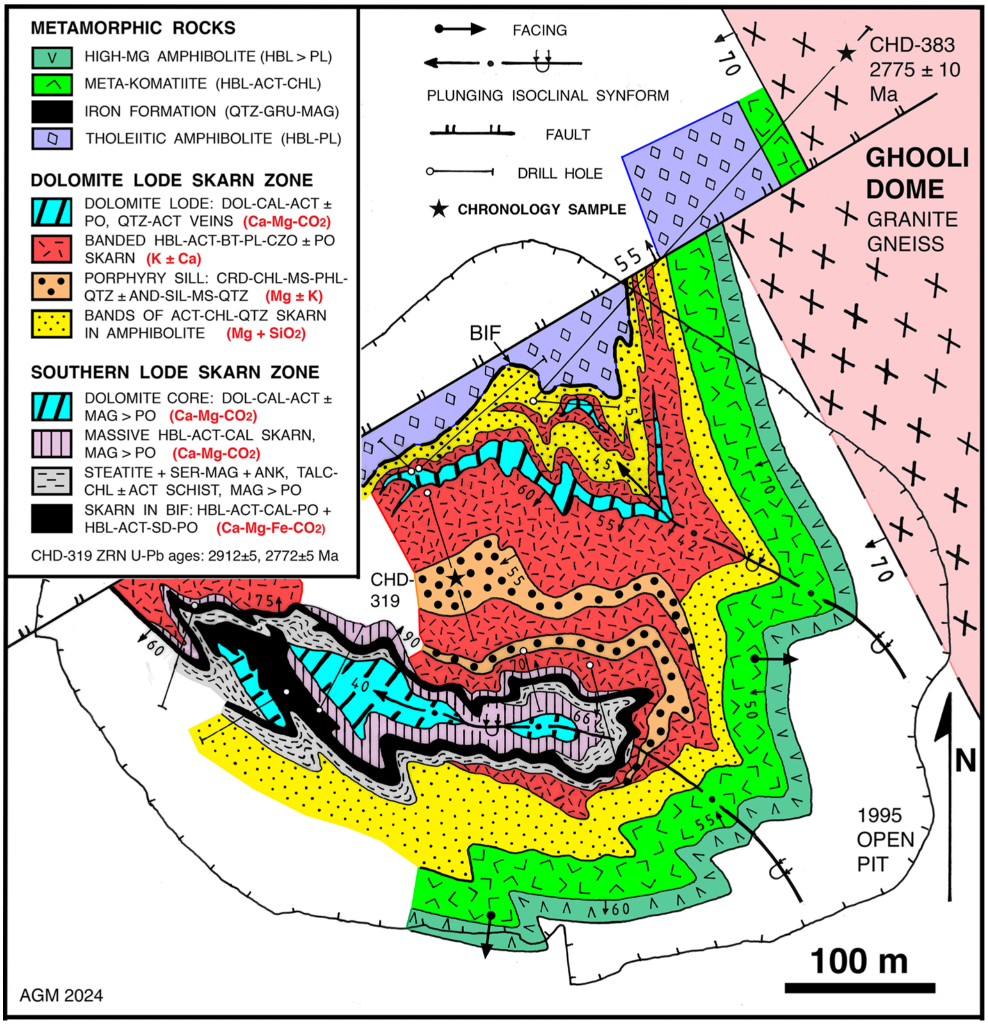

Fig. 6 Geologic map of the Copperhead gold skarn deposit projected onto the 4 level (125 m below surface) of the 1952 Main shaft (modified from Mueller and McNaughton 2000). The lateral evolution of metasomatism (Table 2) away from the main ore body, the Dolomite Lode, is apparent in juxtaposed felsic and mafic precursor rocks. Zircons from one quartz porphyry sill (drill core CHD-319) and from the Ghooli Dome granite gneiss (CHD-383) gave concordant U-Pb ages dating sill emplacement (2912 ± 5 Ma), pre-skarn amphibolite-facies contact metamorphism in the sill (2772 ± 5 Ma), and granite emplacement in the Ghooli Dome (2775 ± 10 Ma; Mueller and McNaughton 2000)

of banded hornblende-biotite-plagioclase skarn (Fig. 6). Hornblende bands with actinolite selvages alternate on a cm-scale with biotite-plagioclase-quartz bands. The hornblende bands and late quartz-actinolite veins contain native gold attached to pyrrhotite (1 vol%). Calcic plagioclase is partly altered to clinozoisite. The biotite-rich skarn grades outward into a quartz-rich zone of actinolite-chlorite alteration with lenses of remnant amphibolite, which is in contact with least-altered meta-komatiite (Fig. 6).

Two altered sills of quartz porphyry are intercalated with hornblende-biotite-plagioclase skarn. They are characterized by two mineral assemblages: (1) cordierite porphyroblasts in a fine-grained matrix of chlorite + muscovite + phlogopite + quartz and, (2) andalusite porphyroblasts in a matrix of muscovite + quartz + sillimanite. The dominant chlorite-cordierite assemblage alternates with and grades into muscovite-aluminosilicate domains. Carbonates are accessory or absent. Zircons samples from one sill and from the Ghooli Dome orthogneiss (Fig. 6) gave concordant U-Pb ages dating sill emplacement at 2912 ± 5 Ma, and recrystallization of metamict zircons at 2772 ± 5 Ma in the amphibolite-facies aureole of the batholith (Mueller and McNaughton 2000).

Dolomite Lode The Dolomite Lode is controlled by folded foliation planes oriented parallel to the lithologic contacts. The ore is composed of dolomite (50–60 vol%) crosscut by folded, irregularly networked, and oriented actinolite veins (20–25%) with selvages of ferroan calcite (10–15%), accessory chlorite and biotite. The actinolite-calcite veins are selectively mineralized with disseminated pyrrhotite (0.5–5%), trace chalcopyrite and native gold (in actinolite), and locally enclose cores of granular quartz (Fig. 7a). Late quartz veins zoned to actinolite rims, most 1–15 cm thick and oriented NNE/15–55° SE, also contain pyrite, galena and scheelite. They are enriched in native gold, and were plated with native silver in the oxidation zone (Blatchford and Honman 1917).

Southern Lode The Southern Lode synform in BIF (Fig. 6) is composed of central dolomite-actinolite-calcite skarn similar to the Dolomite Lode, and outer hornblende-calcite

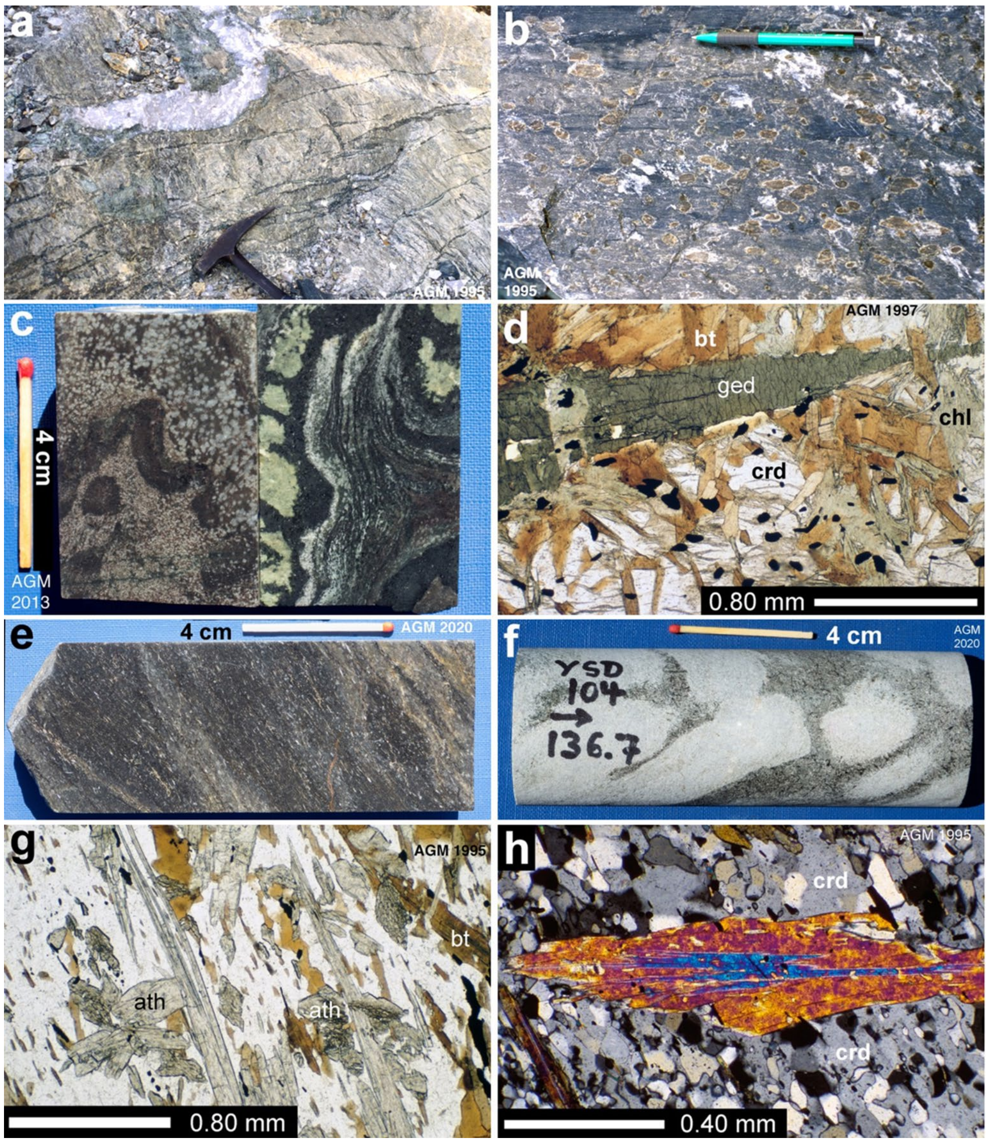

Fig. 7 Calcic skarn, chlorite-cordierite, and anthophyllite-cummingtonite alteration in gold skarn deposits of the Southern Cross Belt. **(a)** Copperhead, Dolomite Lode: a quartz-actinolite vein and green actinolite bands crosscut light grey dolomite + calcite, open pit, the hammer head is 17 cm. (**b**) Copperhead, quartz porphyry: brown cordierite porphyroblasts in a groundmass of chlorite + muscovite + phlogopite + quartz, open pit, the pen is 14 cm. **(c)** Nevoria, BIF-1 contact skarn in amphibolite: LEFT, grey anthophyllite and brown biotite in quartz + anorthite spotted by zoisite + muscovite; RIGHT: green diopside zoned to dark green hornblende + white plagioclase and outer biotite, drill hole DDH-2, 116.5 m, 130.4 m. **(d)** Nevoria, BIF-1 contact skarn: gedrite (ged) + biotite (bt) + cordierite (crd, pinitized along cracks) ± quartz, opaque magnetite + ilmenite, retrograde chlorite (chl), drill hole NGM-9A, 189 m, plane polarized light. **(e)** Yilgarn Star, skarn in amphibolite at graphitic schist: anthophyllite-cummingtonite-cordierite-plagioclase-quartz ± biotite rock, grey anthophyllite (5 mm), minor pyrrhotite (5%). Drill hole YSD-104, 127.0 m. **(f)** Yilgarn Star, lineated skarn between graphitic schist: white-grey cummingtonite-plagioclase ± quartz skarn and interstitial green hornblende. YSD-104, 136.7 m. **(g)** Yilgarn Star, contact skarn: anthophyllite (ath) + biotite (bt) in colourless quartz, plagioclase (An46), and accessory cordierite. YSD-104, 127.0 m, PPL. **(h)** Yilgarn Star skarn: cummingtonite needles (blue) in anthophyllite (orange-red) in contact with quartz and cordierite (crd). YSD-104, 127.0 m, crossed polars

skarn, steatite-dolomite-serpentine "soapstone" and talc-chlorite schist, all mineralized with disseminated magnetite (1–5 vol%) and minor pyrrhotite. The presence of magnetite contrasts with the absence of this oxide in the Dolomite Lode. Gold ore is confined to quartz-grunerite-magnetite BIF replaced by massive, net-textured, and breccia hornblende-actinolite-calcite and actinolite-siderite skarn rich in pyrrhotite (5–15 vol%).

Metasomatism The lateral zonation of skarn-related metasomatism in the Copperhead deposit is particularly apparent in the whole-rock geochemical data (Table 2). First of all, the near-zero TiO_2 and very low Zr contents of the Dolomite Lode indicate that this ore body formed by accretion in dilated foliation planes. The composition of the ore thus reflects strong carbon dioxide, calcium and magnesium metasomatism. If structural relations in the ore body are taken into account, the infiltrating Mg-Ca-CO_2 fluid evolved to a more ferrous composition during the formation of late actinolite-calcite-pyrrhotite veins. In outer hornblende-biotite replacement skarn, potassium is enriched. Calcium enrichment is not obvious but the abundance and calcic composition of plagioclase and clinozoisite are reflected in the high Al_2O_3 content and the CaO/Na_2O ratio of this skarn. The analyses of the altered quartz porphyry sills reveal a striking enrichment in magnesium relative to least-altered granite gneiss (Table 2). Potassium metasomatism remains cryptic due to elevated K_2O in the precursor porphyry.

PTX of skarn formation The Copperhead alteration assemblages, especially those in the quartz porphyry sills (Fig. 7b), place PTX constraints on skarn formation. The dehydration reaction:

$$\text{chlorite} + \text{muscovite} + 2\,\text{quartz} = \text{cordierite} + \text{phlogopite} + 4\text{H}_2\text{O} \quad (1)$$

Table 2 Whole-rock analyses of metamorphic and altered rocks from the Copperhead Au-Ag skarn deposit, Southern Cross Belt, and of granite gneiss in the Ghooli Dome batholith (Fig. 6)

	Metamorphic rocks		Copperhead skarn zones			Quartz porphyry sills		Ghooli Dome
	Meta-komatiite	High-Mg amphibolite	Dol-act-cal ore body	Dol-act-cal ore body	Outer hbl-bt-pl	Crd porphyroblasts in qtz-chl-ms-phl matrix		Biotite granite gneiss
Sample	Pit SS-6	Pit SS-5	210 ft level	Pit SS-7	Pit SS-3	Pit SS-4	CHD-319	CHD-383
Metasomatic enrichment			Ca-Mg-CO_2	Ca-Mg-CO_2	K±Ca	Mg±K	Mg±K	
SiO_2 (wt%)	46.10	48.90	15.83	5.92	56.00	73.80	73.46	73.06
TiO_2	0.31	0.47	0.02	<0.01	0.65	0.23	0.26	0.17
Al_2O_3	6.72	11.30	0.29	0.30	15.60	13.90	12.84	13.97
Fe_2O_3	as FeO	as FeO	0.11	as FeO	as FeO	as FeO	as FeO	as FeO
FeO	9.90	10.44	5.23	6.09	7.29	1.76	2.30	1.41
MnO	0.15	0.16	0.27	0.18	0.08	<0.01	0.02	0.03
MgO	22.30	13.40	17.21	17.00	6.08	3.19	5.23	0.39
CaO	7.58	9.61	27.64	29.00	8.04	0.17	0.55	1.55
Na_2O	0.15	1.42	0.18	0.01	0.34	0.19	0.29	3.64
K_2O	0.03	0.14	0.06	0.06	2.45	3.50	2.27	4.17
P_2O_5	0.01	0.03	0.07	0.01	0.05	0.10	0.10	0.05
LOI	6.98	3.65	32.98	42.53	3.57	2.94	2.48	0.77
Total	100.23	99.52	99.89	101.10	100.15	99.78	99.80	99.21
CO_2	0.01	0.05	31.99	41.70	<0.01	<0.01	1.04	0.14
Sulfur	<0.01	0.01	0.19	0.08	0.62	0.05	0.02	0.02
H_2O	6.97	3.59	0.80	0.75	2.95	2.89	1.42	0.61
Au (ppb)	2	6	960	37	3	<1	n.a.	n.a.
As (ppm)	<1	2	n.a.	4	1	3	<2	<2
Cr	3540	1450	n.a.	10	484	15	21	5
Cu	23	43	n.a.	19	75	14	<2	<2
Ni	760	374	n.a.	100	138	28	25	<1
Pb	<10	<10	n.a.	<10	11	<10	8	31
V	121	187	n.a.	3	249	19	25	14
Zn	82	92	n.a.	46	43	9	15	30
Zr	28	36	n.a.	11	52	183	152	123

Major oxides by XRF fused glass disc, CO2 and sulfur by Leco furnace, loss-on-ignition at 1000 °C, all other trace elements by XRF pressed-powder pellet, Au by fire assay, n.a. not analysed

Data: Dolomite Lode 210 feet level by wet chemical analysis in Blatchford and Honman (1917). CHD drill core analyses from Mueller and McNaughton (2000), all other whole-rock analyses this study has been calibrated experimentally by Seifert (1970) for the KMASH system. This reaction intersects the andalusite-sillimanite phase boundary of Bohlen et al. (1991) at 575 °C and 3.6 kbar (360 MPa) pressure (Fig. 8a). Though sillimanite in the sills is needle-shaped, the Al-silicate phase diagram of Bohlen et al. (1991) is preferred because the pressure estimate is compatible with those obtained for other gold skarn deposits (300–400 MPa) in the SCB. Kyanite is absent at Copperhead.

These PT estimates are supported by thermodynamic calculations using the microprobe analyses in ESM Table 7a plus pure andalusite, sillimanite, quartz and water, the program THERMOCALC 3.26, and the thermodynamic dataset of Holland and Powell (1998; vs. 5.5 updated 2003). Multiple equilibrium calculations (Powell and Holland 1994) resulted in an average temperature of 572 ± 16 °C and pressure of 4.1 ± 0.4 kbar (2-sigma). The sigma-fit (square root MSWD) was slightly above the 95% confidence limit (1.56 > 1.42) but all other quality control parameters remained within acceptable limits. If the results for the Mg-endmember reaction (Fig. 8a) are taken into account, the peak PT-conditions of hydrothermal alteration in the porphyry sills are estimated at 360–410 MPa and 575 °C.

Alteration assemblages in the Southern Lode synform suggest a lateral decrease in temperature and mole fraction CO_2 in the fluid away from the central dolomite-actinolite-calcite skarn. Disseminated dolomite and serpentine aggregates in steatite indicate fluid temperatures of less than 470 °C at 300 MPa and a mole fraction CO_2 of less than 0.1 (Fig. 5.8 in Bucher and Frey 2002). In BIF-hosted reduced skarn, siderite in contact with quartz mesobands has an upper stability limit of 425 °C at X_{CO2} = 0.10 given 400 MPa pressure (Fig. 4b in Miyano and Klein 1989) according to the decarbonation reaction:

$$7\,\text{siderite} + 8\,\text{quartz} + \text{H2O} = \text{grunerite} + 7\text{CO}_2 \qquad (2)$$

Subcalcic amphiboles and outer olivine in skarn

At Nevoria, zones with subcalcic amphiboles in calcic-potassic diopside-biotite skarn (Fig. 7c) replacing amphibolite may be subdivided into three petrographic types: (1) anthophyllite and/or cummingtonite + biotite ± almandine in a matrix of calcic plagioclase (up to An97) + quartz (Fig. 7c); (2) gedrite + biotite + cordierite ± quartz ± almandine ± tourmaline (Fig. 7d), and (3) cummingtonite + plagioclase. Assemblage 1 formed at 586 ± 50 °C and 300–400 MPa in the BIF-1 contact zone (Mueller et al. 2004).

Alteration assemblages characterized by Mg-Fe amphiboles also occur in the outer parts of the Yilgarn Star and Cornishman gold skarn deposits (ESM Figs. 2 and 3). At Yilgarn Star, such replacement occurs in amphibolite (Fig. 7e and f) at the contact and between beds of graphitic quartz-biotite schist located 330 m in the hanging wall of

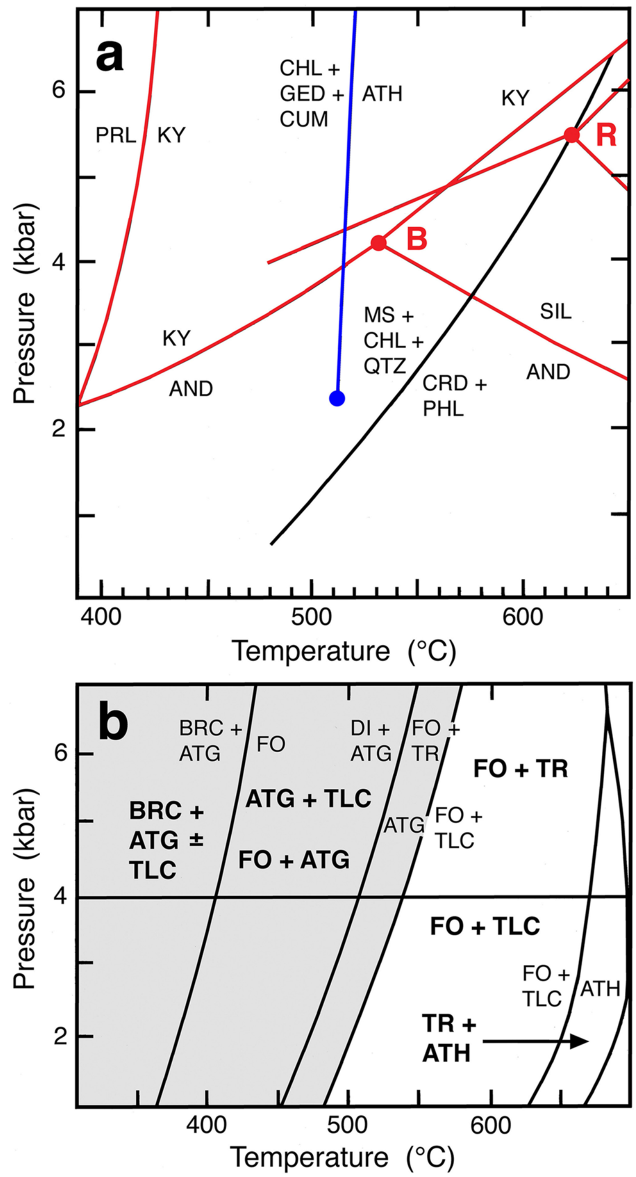

Fig. 8 Pressure-temperature diagrams (1 kbar = 100 MPa) constraining the stability of chlorite-cordierite, anthophyllite- and serpentine-bearing alteration assemblages in gold skarn deposits of the Yilgarn Craton. (**a**) Diagram showing the intersection of the reaction muscovite + chlorite + quartz = cordierite + phlogopite + H_2O in the KMASH system (Seifert 1970) with the aluminosilicate phase boundaries (red lines) linked to the triple points B (Bohlen et al. 1991) and R (Richardson et al. 1969), respectively. The lower thermal stability limit of anthophyllite (blue line) above the invariant point at 220 MPa is based on the empirical grid in Spear (1993: 482). (**b**) Diagram for ultramafic rocks in the CMASH system (modified from Bucher and Frey 2002) showing the stability field (grey) of serpentine (antigorite, lizardite), and of anthophyllite + tremolite. The mineral assemblages in bold may include Mg-chlorite as an additional phase

the magnesian ore skarn. In the contact zone, both anthophyllite and cummingtonite are in equilibrium with calcic plagioclase (An46), cordierite and quartz (Fig. 7g and h). As THERMOCALC average PT calculations gave no result using the microprobe analyses in ESM Tables 7a and 7b, a model endmember set was run for the Yilgarn Star anthophyllite-cordierite-plagioclase assemblage (YSD-104, 127.0 m) including metasomatic hornblende from 136.7 m. The pale green hornblende between the cummingtonite domains (Fig. 7f) encloses cores of dark olive-green hornblende interpreted as the original metamorphic amphibole in contact with andesine (An32-35). For average temperature, four reactions gave a least squares result of 504 ± 72 °C (2-sigma) and a sigma-fit of 1.17 significant at the 95% confidence level (< 1.61). The temperature estimate is broadly consistent with the lower stability limit of 510–520 °C for anthophyllite based on the empirical reaction (Fig. 8a):

$$\text{chlorite} + \text{gedrite} + \text{cummingtonite} = \text{anthophyllite} + H_2O \quad (3)$$

Outer olivine Poikilitic olivine porphyroblasts partly retrograded to serpentine + magnetite in ultramafic amphibole-chlorite rock mark the outer "spotted" alteration zone of the Nevoria (Fig. 4b) and other gold skarn deposits in the SCB. The magnesium metasomatism apparent in the altered quartz porphyry sills at Copperhead suggests that the outer olivine is hydrothermal in origin. The selective replacement of the olivine by serpentine + magnetite indicates that the fluid temperature fell to less than 540 °C, and probably to < 400 °C at 400 MPa pressure (Fig. 8b) given an estimated ambient temperature of 350 °C at 15 km crustal depth.

Mt Marion-Wattle Dam Au-Li district

The Mt Marion-Wattle Dam and Pioneer Dome Au-Li ± Cs districts are located in the Kalgoorlie Terrane close to the boundary the Lake Johnston granite batholith forms with the EG orogen (Fig. 1). The deposits occur in 2.7 Ga greenstones of the upper Kalgoorlie Group komatiite-basalt and the Black Flag Group dacite-greywacke successions folded into tight regional anticlines and synclines (Mueller et al. 2020). The greenstones are contact metamorphosed in the 10–15 km wide aureole of the batholith and its outlier domes. An inner upper amphibolite-facies zone (650–600 °C) grades east into one of lower amphibolite facies (560–530 °C), both formed at 400 MPa isobaric pressure (Bickle and Archibald 1984).

The Mt Marion-Wattle Dam district (Fig. 9a) includes the Mt Marion Li-pegmatite mine, and several prospects marked by outcrops of spodumene pegmatite and drill hole plus soil geochemical anomalies (0.8–5.0% Li_2O, 80–230 ppm Sn, 20–350 ppm Ta, 50–125 ppm Cs; Kalamazoo Resources 2024; Maximus Resources 2024). Anthophyllite is a major gangue mineral in gold ore at Ghost Crab and Spargoville, and part of porphyry-related wall-rock alteration at two komatiite-hosted Ni-Cu deposits. At Wattle Dam, a sodic gedrite-gold assemblage overprints calcic-potassic hornblende-biotite-carbonate skarn.

Ghost Crab gold deposit

The surface footprint of the Ghost Crab deposit consisted of three linear gold anomalies in soil at meta-greywacke-komatiite contacts (Fig. 9b), and of a circular magnetic anomaly centered on the southern trend (Miller et al. 1999). The overturned lithologic contacts dip 60–65° NE close to the Depot granodiorite dome (2689 ± 3 Ma; ESM Table 1), but are sub-vertical further northeast at Mt Marion. The Mt Marion pegmatite dikes dip 10–30° west towards the gold anomalies (Fig. 9b). The western aplite-pegmatite complex thickens with depth to 223 m at 1.6% Li_2O (Smith and Ross 2017) perhaps pointing to a deep granite further west. A few pegmatite dikes, weakly mineralized with gold, were encountered in the Ghost Crab ore body (Miller et al. 1999). The open pit yielded 0.410 Mt at 4.2 g/t Au (1997–1999). The Main Lode was stratabound to a single paragneiss unit 10–40 m thick. The ore shoot plunged 50° NW and was mined to 800 m below surface, where the West Lode was discovered and partly stoped (Fig. 9c). The underground ore had head grades of 4.7–4.9 g/t Au (Miller et al. 1999).

Metamorphic rocks At least six beds of paragneiss, interpreted as metamorphosed sand- and siltstone turbidites, are intercalated with the mine volcanic succession (Fig. 10). The paragneiss units are composed of biotite (5–20 vol%), granoblastic quartz + plagioclase (70–80%), and trace amounts of micron-sized graphite. The plagioclase is close to andesine in composition (An30). The northeast gneiss is leucocratic (5–10% biotite) and contains recrystallized detrital quartz and lithic clasts indicating a psammitic precursor. The other gneiss beds are biotite-rich (15–20%), and contain bands of cordierite (10–15%) and post-kinematic porphyroblasts (1–5%) of garnet, staurolite (Fig. 11a), and rare andalusite.

The volcanic succession comprises meta-komatiite (> 18 wt% MgO; >2000 ppm Cr), minor high-Mg amphibolite, and thin interflow graphitic chert. The meta-komatiites consist of hornblende, actinolite, and Mg-rich chlorite, and are foliated parallel to lithologic contacts. The amphiboles are randomly oriented on chlorite foliation planes (Fig. 11b). The amphibolites are composed of hornblende and calcic plagioclase (>An30).

Outer anthophyllite alteration Alteration zones (0.1–0.5 m thick) of anthophyllite-cummingtonite-quartz-plagioclase granofels occur in paragneiss interbedded with

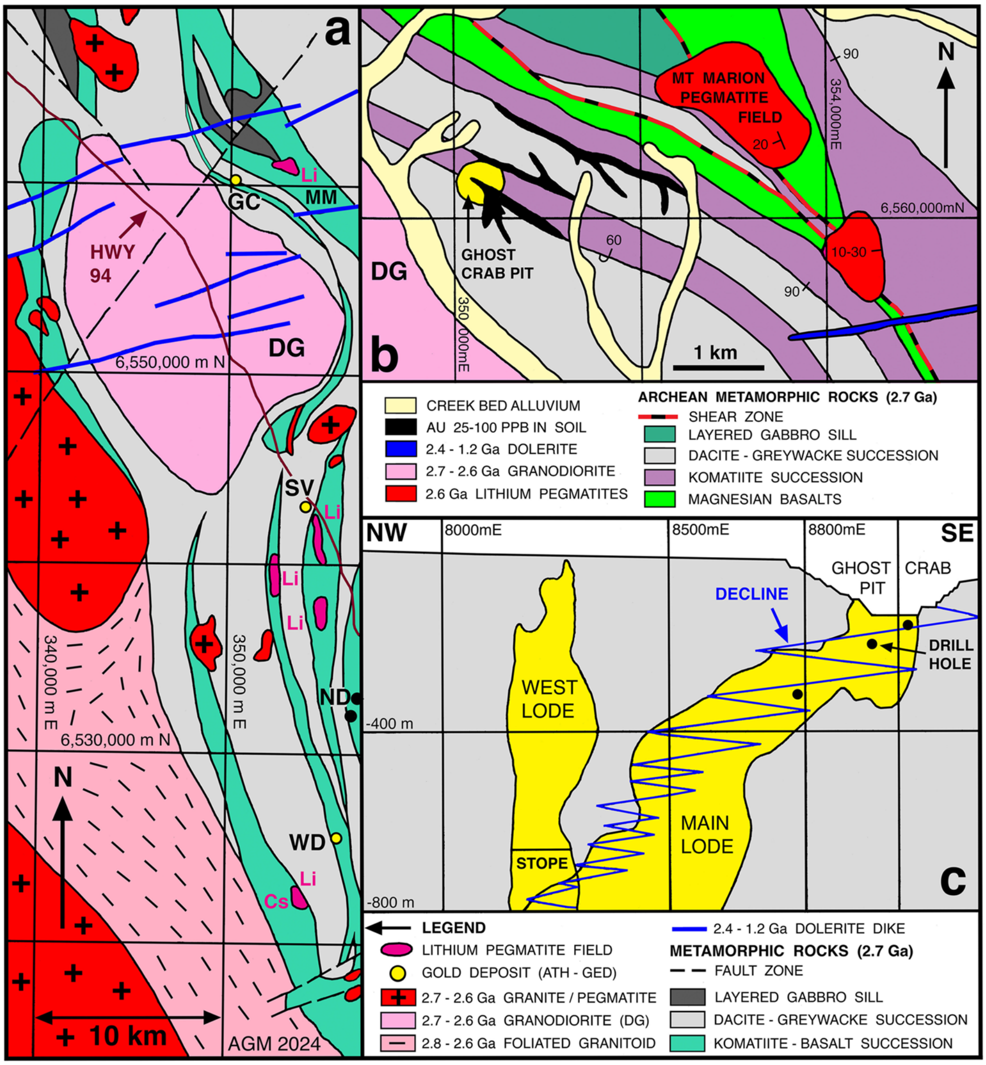

Fig. 9 Granite-pegmatite-skarn spatial relations in the Mt Marion-Wattle Dam Au-Li district, Kalgoorlie Terrane, Eastern Goldfields orogen. (**a**) District geologic map (modified from Hunter 1988) showing the Mt Marion spodumene pegmatite mine (MM), lithium prospects defined by pegmatite outcrops and Li-Cs-Ta anomalies (Kalamazoo Resources 2024; Maximus Resources 2024), the Ghost Crab (GC), Spargoville (SV) and Wattle Dam (WD) gold deposits, and the location of porphyry-related anthophyllite-tremolite alteration (ND). (**b**) Geologic map showing the stratabound gold-in-soil anomalies associated with the Ghost Crab deposit, and the outcrop areas of the Mt Marion pegmatites dipping west towards the anomalies (Hunter 1988; Mueller 1997b). (**c**) Longitudinal projection of the Ghost Crab deposit (20.2 t Au; ESM Table 5) showing the open pit, the underground mine, the pierce points in the Main Lode of the diamond drill holes logged, and the partly stoped West Lode ore body (modified from Alacer Gold 2012)

meta-komatiite in the structural hanging wall of the main alteration zone (Fig. 10). These contact zones increase in abundance to the SSW but contain little pyrrhotite (0.5–1%) and are low in gold (<0.05 g/t). The outermost paragneiss units in both the hanging wall and footwall are barren (<0.01 g/t Au) but marked by retrograde muscovite-chlorite bands, by sparse quartz-tourmaline veins, and by spaced zones anomalous in arsenic (10–80 ppm). Drill hole GTC-8800-5 is located at the NW-termination of the middle gold-in-soil anomaly marking the Ghost Crab deposit. The intensity of mineralization at the lithologic contacts of the outer hanging wall paragneiss may thus increase southeast of the cross section in Fig. 10.

Magnesian skarns The altered ultramafic rocks in the hanging wall of the Main Lode are marked by an arsenic anomaly (50–1000 ppm) caused by disseminated arsenopyrite. Magnesian skarns replace meta-komatiite in lens-shaped aggregates, 1–10 cm-thick bands, and in veins and zones oriented parallel to foliation (Fig. 10). Broader zones contain seams of chlorite-talc and phlogopite-talc schist, olivine porphyroblasts (5–15%), and lens-shaped aggregates of olivine+actinolite

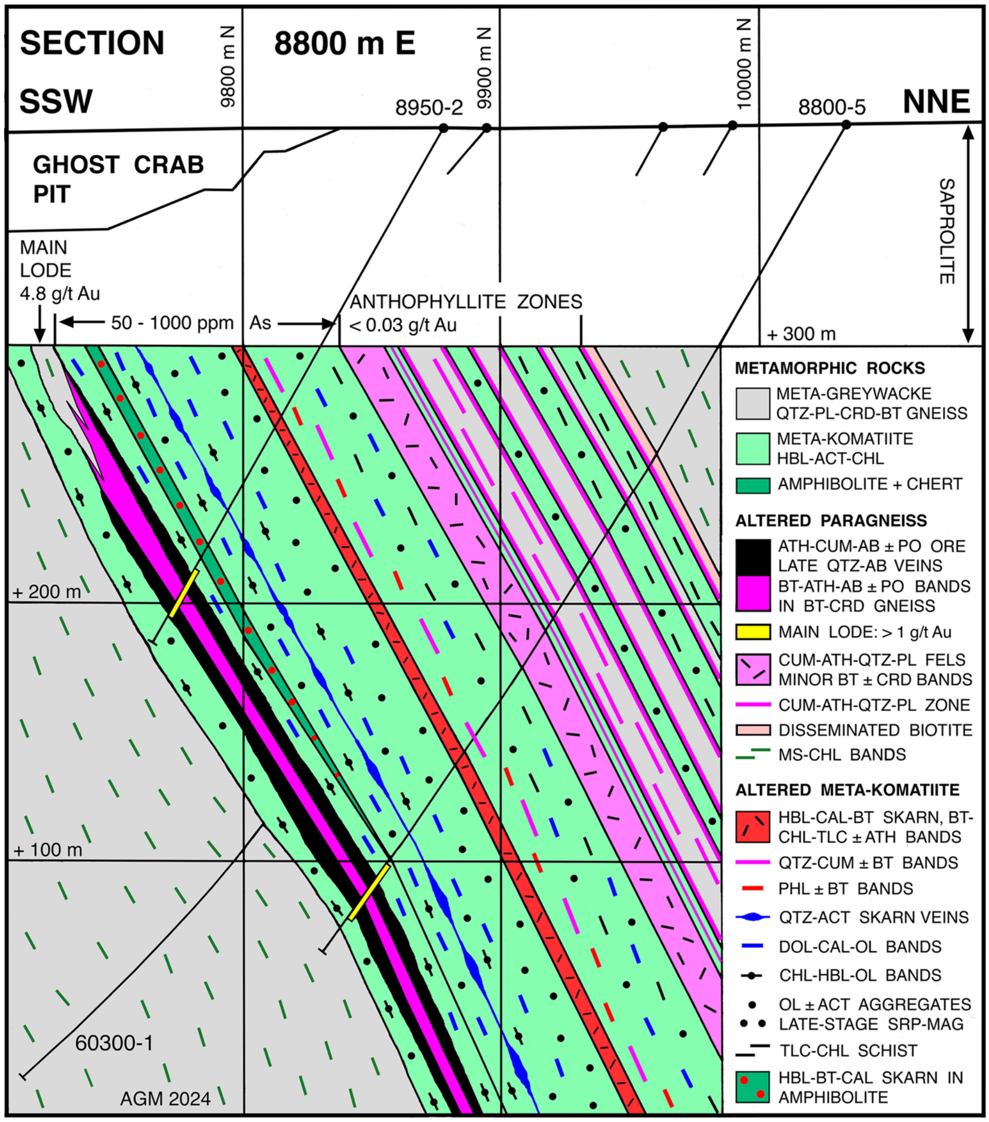

Fig. 10 Cross section at 8800 m mine grid east through the alteration zone of the Ghost Crab gold deposit based on the lithologic logs of drill cores GTC-8800-5, GTC-8950-2 (projected), and GTC-60300-1 (projected), constructed from petrographic data in Mueller (1997b). The gold ore of the Main Lode is bound to the hanging wall and footwall contacts of a single paragneiss bed but extends into adjacent magnesian skarn in meta-komatiite

(5%) and/or olivine + anthophyllite (10–15% locally). Some olivine is post-kinematic and oriented perpendicular to the chlorite foliation. Most is partly replaced by serpentine + magnetite, the cause of the magnetic anomaly at surface.

Pinch-and-swell quartz veins (0.10 g/t Au), up to 90 cm thick, were intersected in a 4 m wide zone. The core of granoblastic quartz is rimmed by fibrous actinolite, minor biotite and dolomite. The zoned vein is enclosed in outer chlorite schist containing post-kinematic hornblende and olivine. Spaced bands of calcic-potassic skarn, composed of hornblende, biotite-phlogopite and calcite (up to 30 vol%), were intersected in meta-komatiite (Fig. 11c) and in intercalated amphibolite. This skarn is associated with talc-chlorite schist containing post-kinematic phlogopite and/or anthophyllite, and with local cummingtonite-quartz replacement.

Olivine-actinolite-dolomite skarn proximal to the Main Lode (Fig. 10) contains minor hornblende, calcite, accessory phlogopite, chlorite and talc, and disseminated pyrrhotite and native gold. In many bands, olivine is a major constituent forming porphyroblasts up to 4 mm long (Fig. 11d). Magnesian skarn at the hanging wall contact of the Main Lode averaged 2–3 g/t gold in drill core. In the footwall, anthophyllite-bearing olivine-actinolite bands (2.2–12.4 g/t Au) are associated with chlorite schist marked by post-kinematic hornblende and olivine. Magnesian contact skarn is

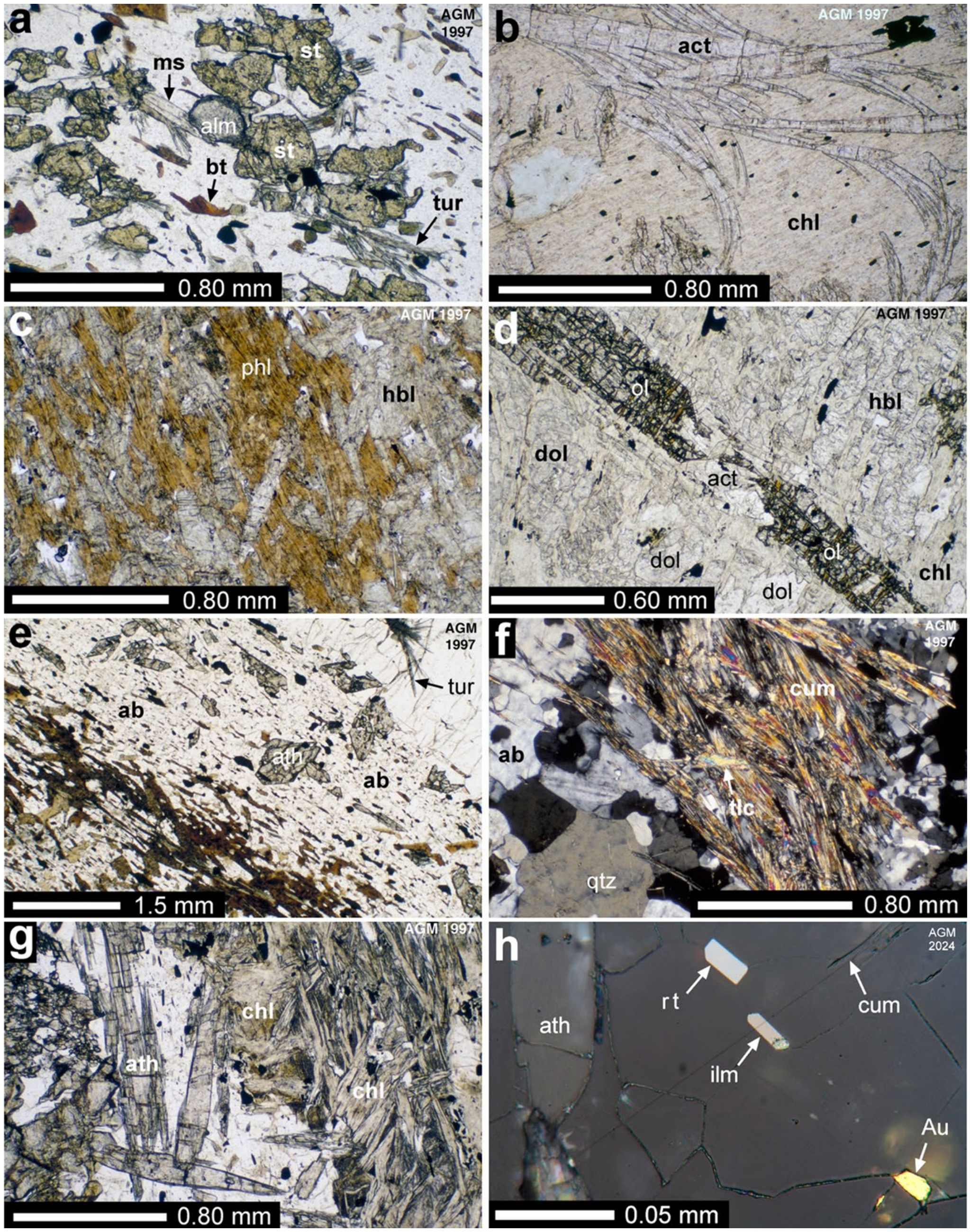

Fig. 11 Photomicrographs of metamorphic and alteration mineral assemblages from the Ghost Crab gold deposit, Kalgoorlie Terrane, Eastern Goldfields orogen. (**a**) Paragneiss: metamorphic almandine (alm), staurolite (st), biotite (bt), muscovite (ms) and tourmaline (tur) in colorless cordierite + quartz. Drill hole GTC-60300-1, 345.6 m, plane polarized light. (**b**) Meta-komatiite: metamorphic actinolite (act) in chlorite (chl), opaque ilmenite and sulfide. GTC-8800-5, 161.4 m, PPL. (**c**) Magnesian skarn (0.05 g/t Au): hornblende (hbl) + phlogopite (phl), interstitial colorless calcite. GTC-8800-5, 292.1 m, PPL. (**d**) Magnesian skarn (0.15 g/t Au): olivine (ol) + actinolite (act) + dolomite (dol) replace hornblende (hbl) + chlorite (chl). GTC-8950-2, 225.3 m, PPL. (**e**) Main Lode (8.6 g/t Au) in paragneiss: Quartz-tourmaline (tur) vein with selvage of anthophyllite (ath) + albite (ab) ± quartz in biotite-cordierite gneiss. GTC-8950-2, 213.0 m, PPL. (**f**) Main Lode (11.1 g/t Au): cummingtonite (cum) + retrograde talc (tlc) in quartz (qtz) + albite (ab). GTC-8950-2, 201.0 m, crossed polars. (**g**) Main Lode (17.8 g/t Au): anthophyllite (ath) and Mg-Fe chlorite (chl) in colourless quartz + albite. GTC-8950-2. 199.3 m, PPL. (**h**) Main Lode: native gold (Au), rutile (rt), ilmenite (ilm), anthophyllite (ath) and cummingtonite (cum) in quartz + albite. GTC-8950-2, 199.3 m, PPL reflected in air

strongly enriched in carbon dioxide, calcium, and strontium relative to least-altered meta-komatiite (Table 3).

Main Lode ore body The anthophyllite alteration zones in biotite paragneiss include the Main Lode mined as one unit above and in separate hanging wall and footwall stopes below 600 m depth (Miller et al. 1999). Drill core analyses indicate that the ore is low in arsenic (5–75 ppm), total base metals (<200 ppm), and silver (0.5–1.6 ppm) resulting in high Au: Ag ratios (5:1 to 10:1).

The up to 6 m thick contact zones (5–15 g/t Au) consist of light grey, fine-grained metasomatic gneiss and granofels. The groundmass of isogranular quartz and albite-oligoclase

Table 3 Whole-rock analyses and CIPW mineral norms of paragneiss, anthophyllite-albite gold ore and magnesian skarn, Ghost Crab deposit, and of skarn-related granite dikes, Chalice deposit, Kalgoorlie Terrane

	Ghost Crab gold skarn deposit			Chalice gold skarn: Granite dikes		
Rock type	Least-altered paragneiss	Gold ore in paragneiss	Magnesian skarn	Least-altered Dike-2	Dike-2 ore	Endoskarn in Dike-1
Assemblage	bt-crd-qtz-pl	ath-cum-pl-qtz	dol-hbl-ol-chl	qtz-ab-mc-bt	ab-bt>mc	ab-di-act
Drill hole	GTC-8800-5	GTC-8950-2	GTC-8950-2	WMD-118	WMD-28	WMD-118
Depth (m)	375.9	201.0	225.2	532.0	101.2	479.5
SiO_2 (wt%)	62.35	60.90	34.84	73.53	74.01	70.08
TiO_2	0.70	0.63	0.29	0.17	0.16	0.22
Al_2O_3	16.27	16.34	5.07	13.73	13.49	15.62
Fe_2O_3	0.00	0.00	0.00	0.30	0.40	0.00
FeO	7.32	6.68	8.94	1.20	1.16	1.38
MnO	0.15	0.10	0.16	0.03	0.04	0.03
MgO	4.28	3.95	24.75	0.43	0.46	0.78
CaO	2.02	1.21	10.00	1.04	1.43	1.31
Na_2O	2.09	7.60	0.12	3.60	4.25	8.16
K_2O	2.57	0.51	0.01	5.30	3.73	1.60
P_2O_5	0.12	0.08	0.04	0.05	0.07	0.08
LOI	1.97	1.71	13.53	0.63	0.88	0.82
Total	99.84	99.71	97.75	100.01	100.08	100.08
CO_2	0.22	0.44	7.88	0.50	0.36	0.89
S	0.33	1.46	0.21	0.05	0.03	0.61
Au (ppm)	<0.01	11.2	0.15	0.01	6.6	0.04
Cr	318	286	2032	<3	5	9
Ni	131	97	1480	2	<1	<1
Rb	97	32	17	234	198	13
Sr	60	294	198	125	159	217
Zr	126	118	21	185	189	156
CIPW norm (cation percent)						
cc	0.58	1.08	19.98	1.28	0.92	2.16
ap	0.27	0.16	−0.06	0.11	0.16	0.16
pr	0.89	3.66	0.54	0.14	0.08	1.52
il	1.00	0.84	0.40	0.24	0.22	0.30
or	15.60	2.90	0.05	31.45	22.20	9.05
ab	19.25	65.60	1.10	32.50	38.45	70.20
an	8.02	2.60	0.00	1.62	4.35	0.35
c	8.05	2.41	5.32	1.62	0.97	0.35
mt	0.00	0.00	0.00	0.32	0.42	0.00
hy	22.41	17.28	81.92	2.56	2.59	2.83
q	23.95	3.47	−9.30	28.16	29.65	13.09
Sum	100.01	100.00	99.95	99.99	100.00	100.00
Correlation of CIPW norm with minerals observed in thin section (vol% estimates)						
hypersthene	bt 15, crd 15, grt 1, st 1	ath 8, cum 10, tlc 0.5, bt 0.5	chl 30, hbl 20, ol 10, dol 30	bt 4, chl 0.5, ep 0.3	bt 4, chl 1, ep 0.2	cpx 10, act 5, bt 1
corundum	bt 15, crd 15,	crd 2–5?	chl 30	bt 4, ms 1	bt 4, ms 1	bt 1

Major oxides by XRF fused glass disc, CO2 and sulfur by Leco furnace, loss-on-ignition at 1000 °C, Au by fire assay, all other trace elements by XRF pressed-powder pellet. Reference values for least-altered Ghost Crab meta-komatiite: 0.18% CO2, 4.89% CaO, 11 ppm Sr. CIPW norm after Barth (1955), normative hematite and diopside were Zero contains 5–10% biotite and 10–15% light grey Mg-Fe amphibole needles (1–5 mm) composed of randomly oriented anthophyllite in plagioclase-rich bands (Fig. 11e), and of cummingtonite in quartz-rich granofels (Fig. 11f). Some anthophyllite crystals enclose cores of cummingtonite. Locally, anthophyllite is in contact with Mg-Fe chlorite (Fig. 11g), and cummingtonite is replaced by rare talc (Fig. 11f). Veins (10–15 vol%) of granular quartz contain accessory Mg-Fe amphibole, biotite and chlorite, and are bordered by anthophyllite-albite replacement selvages (Fig. 11e). The contact zones are mineralized with pyrrhotite (3%), subhedral ilmenite and rutile (1%), trace chalcopyrite, and native gold at silicate (Fig. 11h) and silicate-pyrrhotite grain boundaries. The gold ore is strongly enriched in sodium and sulfur, evident in the increased CIPW normative albite and pyrite, and enriched in strontium relative to least-altered paragneiss (Table 3).

The central part of the Main Lode (5–10 g/t Au above 600 m depth) consists of dark brown, fine-grained gneiss composed of granoblastic quartz and plagioclase, biotite (10–20%), randomly oriented anthophyllite needles (10%; 1–10 mm), and accessory late-stage chlorite. Biotite-anthophyllite gneiss is intercalated on a cm-scale with biotite-cordierite gneiss. Much of the cordierite, pinitized along cracks, may be metamorphic but stable in contact with anthophyllite.

P-T of skarn formation Pressure is constrained by the pre-skarn metamorphic assemblages in the aureole of the Lake Johnston batholith to 400 MPa, and by the syn- or post-gold spodumene pegmatites at Mt Marion to 300–400 MPa. The mutual contacts of anthophyllite with quartz, albite, chlorite, and cordierite (?) suggest a gedrite component. The high-T assemblage gedrite + cordierite + quartz is stable relative to Mg-Fe chlorite + quartz at 550 ± 50 °C (Ernst 1968). The assemblages olivine + tremolite and olivine + talc in magnesian skarn are consistent with this estimate. The retrogression of olivine to serpentine + magnetite suggests a decrease in temperature to about 400 °C (Fig. 8b).

Spargoville gold deposit

The Spargo's Reward mine at Spargoville produced 0.107 Mt of ore at 7.64 g/t Au (0.82 t Au; 1934–1942), and has drill-indicated resources of 0.786 Mt at 4.4 g/t (Corona Resources 2020). The host rocks are sub-vertical dacite breccias and lithic crystal tuffs (2686 ± 3 Ma; Krapez et al. 2000), and greywacke turbidites in a tight regional syncline (Fig. 9a). They are metamorphosed to amphibolite-facies orthogneiss and thin-bedded biotite paragneiss. Pegmatite dikes peripheral to the intrusive complex (1.2–5.0 wt% Li_2O; Kalamazoo Resources 2024) southeast of the gold mine cut the folded succession.

In paragneiss, the more than 80 m wide alteration zone encloses an inner 50 m zone of low-grade gold (0.1–1 g/t), which in turn encloses high-grade ore (8 g/t Au) up to 10 m thick (Fehlberg and Giles 1984). The ore is composed of thin (2–6 cm), closely spaced replacement bands of actinolite-anthophyllite-quartz-carbonate skarn containing arsenopyrite (up to 15 vol%), and minor pyrrhotite, chlorite and titanite. Apart from CO_2, total iron, MgO, CaO and Ce are significantly enriched, Na_2O is depleted, and Cu, Zn and Pb are at background levels relative to least-altered paragneiss (Fehlberg and Giles 1984). The banded skarn grades outward into quartz-sericite-pyrite alteration marked by quartz-muscovite lenses with up to 40% pyrite. Drill holes also intersected an outer pyroxene-plagioclase unit (1.8 wt% As, 0.07 g/t Au), which differs from mafic amphibolite by mineralogy, and by high P_2O_5 (0.87 wt%) and Ce (407 ppm) contents. The Spargoville deposit has been interpreted as volcanic-exhalative (Fehlberg and Giles 1984) but shows similarities to other calcic-potassic replacement skarns.

Porphyry-related skarns

In the 1960s, two small komatiite-hosted Ni-Cu sulfide deposits were discovered south of Spargoville (Fig. 9a). The local volcanic succession dips 70° W, and consists of upper greenschist facies amphibolite, thin flows of tremolite-chlorite meta-komatiite, and thick flows of meta-komatiite with basal lenses of partly serpentinized olivine adcumulate (Andrews 1975). Drill holes intersected several dikes of quartz-albite porphyry, characterized by albitized feldspar megacrysts and accessory biotite. The dikes are associated with calcic endoskarn and meter-scale barren exoskarn bound to the intrusive contacts. In dunite, Ca-Al ± K ± CO_2 metasomatism caused the selective replacement of olivine (91–93 mol% Fo) by inner tremolite-anthopyllite and by outer antigorite-chlorite assemblages. Late-stage calcic hornblende-actinolite ± dolomite contact skarn and outer disseminated phlogopite and talc overprint the early alteration (Hancock et al. 1971). The tremolite-anthophyllite replacement of forsterite indicates a peak fluid temperature of more than 650 °C (Fig. 8b).

Wattle Dam The Wattle Dam gold deposit (Fig. 9a; ESM Table 5) is centered on graphitic interflow chert in a sub-vertical succession of meta-komatiite and high-Mg amphibolite. Quartz-feldspar porphyry dikes emplaced 200 m east of the ore body are part of a steeply west-dipping, 200–250 m thick and 3 km long intrusive complex mineralized with low-grade gold (0.04–0.5 g/t; Ramelius Resources 2012). In the adjacent meta-komatiite, disseminated molybdenite, scheelite and arsenopyrite are spatially associated with the intrusions (Bath et al. 2020).

The high-grade (15–20 g/t Au) main ore body is enclosed in Stage 1 hornblende-biotite-dolomite-calcite ± plagioclase skarn containing disseminated Ce-allanite, magnetite and pyrite. The 100-m-wide hornblende-biotite zone (1.5 g/t Au) grades into outer chlorite-carbonate ± quartz and serpentine ± talc alteration in amphibolite and meta-komatiite, respectively (Bath et al. 2020; Maximus Resources 2024). The calcic-potassic skarn is overprinted by a Stage 2 fracture network lined with an oxidized sodic assemblage composed of gedrite (up to 5000 ppm Cl), minor riebeckite, aegirine, anhydrite, chalcopyrite, Bi-tellurides and native gold. Late veins are filled with calcite and quartz, mineralized with gold, pyrrhotite and pentlandite, and surrounded by biotite-chlorite selvages (Bath et al. 2020).

Pioneer Dome Au-Li-Cs district

The Pioneer Dome 30 km NNW of Norseman is a satellite intrusive complex east of the Lake Johnston batholith emplaced into 2.7 Ga amphibolite-facies greenstones of the Kalgoorlie Terrane. The dome consists of a large raft of orthogneiss at its eastern border (Fig. 12a), dated at 2825 ± 60 Ma by a Rb-Sr total rock age, and of magnetite-series biotite granites dated indirectly at 2664 ± 5 Ma by recrystallized zircons in the orthogneiss (ESM Table 1). Late LCT pegmatite dikes intrude both the granitoids and greenstones, and cluster at the periphery of the dome (Batt et al. 2021). Clusters include spodumene pegmatites at the north end (11.2 Mt at 1.21% Li_2O; Phelps-Barber et al. 2022), and the Mt Thirsty cassiterite pegmatites at the south end (Witt 1992).

The Sinclair open pit mine east of the dome (Fig. 12a) produced 18,629 metric tons of pollucite concentrate at 8.32% Cs_2O in 2018–2019 (Pioneer Resources 2020). The 150 m thick pegmatite is zoned inward from a coarse-grained Wall Zone of albite-quartz-microcline (± garnet, tourmaline), either aplitic or muscovite-rich, to an inner Quartz Zone enclosing a potassic core (11.6% K_2O) of megacrystic perthitic microcline. Below this 35–40 m thick microcline cap are four highly fractionated zones: (1) quartz ± beryl, (2) megacrystic petalite + interstitial eucryptite rimmed by pink cookeite, locally rare amblygonite and spodumene, (3) lepidolite with up to 4.5% Li_2O in bulk rock, minor zinnwaldite and albite, and (4) 2–10 m long lenses of pollucite with up to 29% Cs_2O (Crook et al. 2019; Batt et al. 2021).

The Chalice skarn deposit is located in the narrow belt of amphibolite and meta-komatiite separating the Lake Johnston batholith from the Pioneer Dome (Fig. 12a). The mine produced 3.9 Mt of sulfide ore at a recovered grade of 4.7 g/t Au (1995–1999) from open pit and underground operations (ESM Table 5). The deposit is of particular interest because of the genetic link between multiple granite-pegmatite emplacement and gold mineralization.

Chalice skarn ore bodies

The Chalice main ore body is hosted by a 150 m thick unit of tholeiitic amphibolite foliated parallel to the contacts with intercalated meta-komatiite. Hornblende-plagioclase thermobarometry indicates metamorphic conditions of 500–550 °C and 400 MPa pressure (Bucci et al. 2002). The succession strikes NNW and dips 65–70° west, where the border granite of the Lake Johnston batholith intrudes a mafic-ultramafic lithologic contact (Fig. 12b). To the east, the amphibolite is intercalated with meta-komatiite marked by olivine porphyroblasts retrograded to serpentine + magnetite.

The main ore body (5–6 g/t Au, 2.5 g/t Ag) is lens-shaped in cross section (Fig. 12b) and plunges 50° NNW (Mueller 1997c). The skarn is composed of foliation-parallel, closely spaced replacement bands of diopside-oligoclase ± epidote zoned to outer hornblende (Fig. 13a), minor grossular-andradite-quartz zoned to outer diopside (Fig. 13b), hornblende-actinolite-oligoclase ± biotite, and calcite-biotite. The predominant feldspar is albite-oligoclase (An 05-15). Calcite is widespread but minor. Retrograde minerals confined to the skarn bands are sericite ± prehnite after plagioclase and epidote after garnet. Native gold occurs enclosed in diopside, hornblende and plagioclase, interstitial to garnet, and associated with magnetite (1 vol%), pyrite + pyrrhotite (2–10%), accessory chalcopyrite, and scheelite. The bulk composition of the ore is calcic-sodic rather than calcic-potassic. Cu, Bi and W are geochemically enriched (Mueller 1997c; Bucci et al. 2002). The main ore body grades along and across strike into uneconomic (< 1 g/t Au) skarn-banded amphibolite.

A unit of magnesian skarn (1–2 g/t Au), characterized by abundant calcite (50–60 vol%), is located in the footwall of the main ore body (Fig. 12b), probably replacing thin meta-komatiite. Calcite-phlogopite-chlorite schist containing disseminated magnetite (3–5%) and iron sulfides (1%) alternates with calcite-olivine-chondrodite domains. The olivine is partly retrograded to serpentine and the chondrodite to talc ± serpentine (Mueller 1997c; Bucci et al. 2002).

Chalice granite complex

Gold skarn from the main ore body has been dated by a titanite U-Pb age at 2644 ± 8 Ma, the western border granite by a zircon age of 2631 ± 10 Ma, endoskarn in Dike-1 by a titanite age of 2623 ± 5 Ma, granite Dike-2 by a zircon age of 2626 ± 9 Ma, and a late granite-pegmatite dike by a titanite age of 2622 ± 13 Ma (Bucci et al. 2004). Foliation-parallel skarn in the ore bodies is crosscut by the intrusive complex (average: 2625 Ma) and may be 15–20 Ma older. The U-Pb ages of all granite intrusions agree within error but the dikes of the border pluton may be subdivided according to cross-cutting relationships, alteration style, and intensity of gold

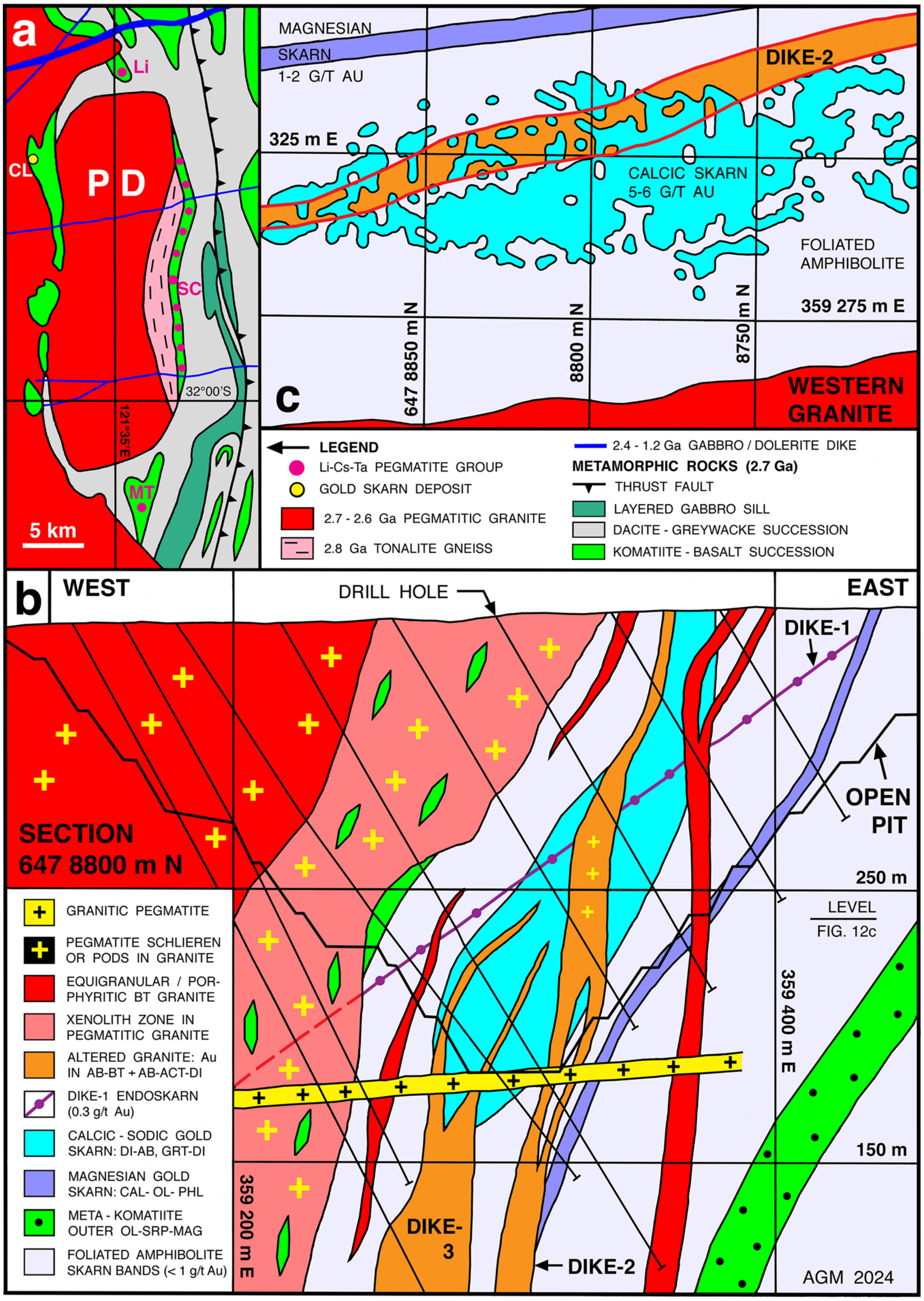

Fig. 12 Ore deposits in the Pioneer Dome Au-Li-Cs district, Kalgoorlie Terrane, Eastern Goldfields orogen. (**a**) District geologic map (modified from Cox and Tyrwhitt 1975; Swager et al. 1995) showing the Chalice (CL) gold mine, the spodumene pegmatites at the north end, the Sinclair (SC) cesium mine and pegmatite prospects at the east margin, and the Mt Thirsty (MT) cassiterite pegmatites at the south end of the Pioneer Dome (PD). (**b**) Cross section at 647,8800 m north (Map Grid Australia) through the Chalice gold deposit (modified from Mueller 1997c) showing the skarn ore bodies in amphibolite and meta-komatiite, and the syn- to post-gold dikes associated with the western granite-pegmatite pluton. **(c)** Open pit plan at 240 m RL showing the distribution of high-grade gold in granite Dike-2

mineralization (Fig. 12b and c). The altered auriferous dikes (Dike-1 to −3) are described below, and other barren members of this suite in Bucci et al. (2002).

The least-altered parts of the intrusions are grey, plot in the monzogranite field by modal mineralogy (20–30% quartz, 5% biotite), and display negative Eu anomalies in chondrite-normalized REE diagrams (Bucci et al. 2002). The western pluton has an equigranular magmatic texture, whereas the microgranite dikes are porphyritic due to zoned plagioclase and minor microcline phenocrysts (Fig. 13c). Quartz-feldspar myrmekitic intergrowth occurs in the groundmass. The border granite is characterized by variable molar Na_2O/K_2O ratios (1.05–3.03), by hematite-stained pegmatite segregations (Fig. 13d), by red granular microcline-quartz ± pyrite replacement bands, and by quartz-feldspar ± calcite filled fractures surrounded by sericite-chlorite selvages. Magnetite (0.5 vol%) and pyrite (0.1–1%) are disseminated in spaced zones. Xenoliths of ultramafic amphibole-chlorite rock are partly replaced by phlogopite, minor talc and magnetite, and by rare pyrite, carbonate, and serpentine. Amphibolite xenoliths are altered to biotite, minor epidote, and pyrite. Segregations of pegmatite are more abundant in the xenolith zone (Fig. 12b), and biotite-pyrite aggregates (10 mm) are present close to the greenstone contact.

Dike 1 Granitic dikes 0.5–3 m thick and completely altered to endoskarn (Dike-1 in Table 3) dip at moderate angles west (30–60°). Some may persist as microgranite (?) into the main pluton. Endoskarn consists of albite-oligoclase (70 vol%), interstitial quartz and microcline (remnant?), diopside-actinolite aggregates and bands (Fig. 13e), and accessory (0.5–1.5%) calcite, titanite, chlorite, pyrrhotite and pyrite (Mueller 1997c). Endoskarn dikes (up to 0.29 g/t Au), some gently folded, were mapped in the open pit where they are crosscut by Dike-2 (Bucci et al. 2004).

Dike-2 Dike-2 is 4–17 m thick, crosscuts the amphibolite-hosted gold skarn sub-parallel in strike to the intrusive contact of the western pluton, and dips 70–80° west (Fig. 12b). North of the open pit, this dike is barren (<0.01–0.03 g/t Au) and located east of the main ore body. It consists of grey porphyritic microgranite (Fig. 13c) containing biotite (5%) and magnetite (0.5%). White-grey quartz-microcline

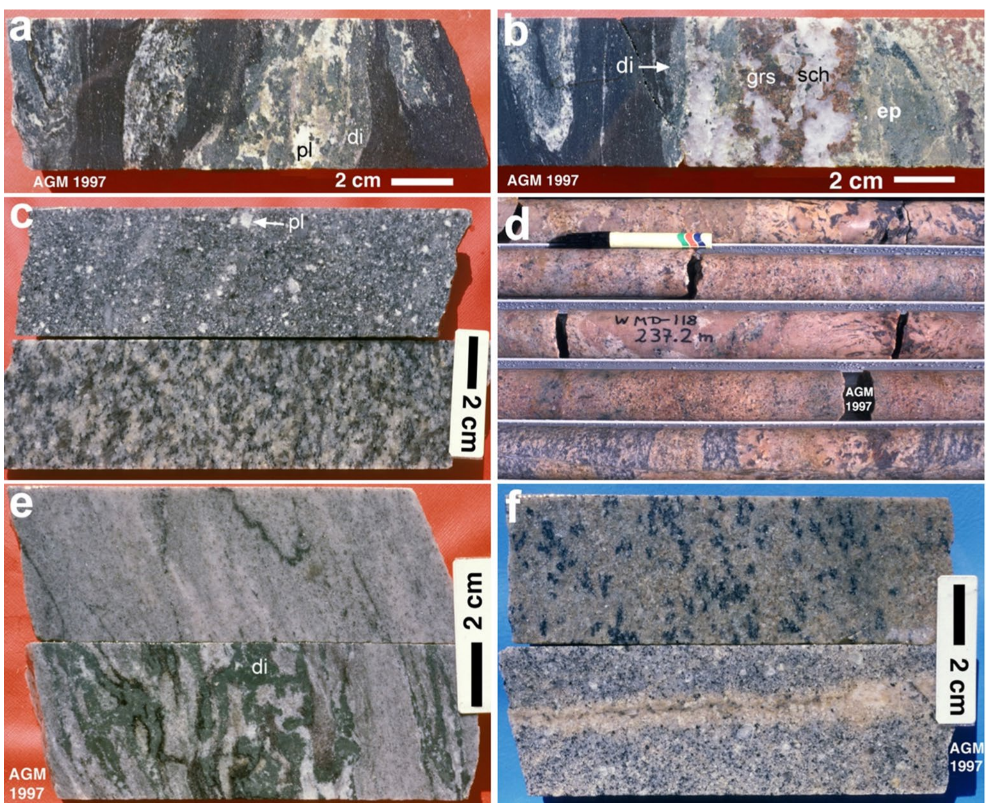

Fig. 13 Drill-core photographs of amphibolite-hosted gold skarn (a, b) and of least-altered and altered dikes associated with the western pegmatitic biotite granite (c-f), Chalice deposit, Kalgoorlie Terrane. (**a**) Gold skarn: diopside (di), oligoclase (pl) partly retrograded to sericite ± prehnite, and yellow epidote zoned to outer hornblende; drill hole WMD-33, 197.5 m. (**b**) Gold skarn: Grossular (grs) + scheelite (sch) + quartz + retrograde epidote (ep) zoned to outer diopside (di); WMD-33, 211.5 m. (**c**) Least-altered granites: TOP: Microgranite with zoned plagioclase (pl) phenocrysts, Dike-2, WMD-118, 532.0 m; BOTTOM: Western biotite granite with equigranular texture, WMD-118, 275.1 m. (**d**) Pegmatitic granite: oxidized zones of graphic biotite pegmatite and intercalated aplite in grey granite; WMD-118, 235–239 m. **(e)** Dike-1 endoskarn (0.01–0.29 g/t Au): disseminated actinolite (black-green), diopside, pyrite (1%) and pyrrhotite (1%); zoned bands of diopside (di) + actinolite in white-grey albite-oligoclase ± quartz; WMD-118, 479.5, 479.9 m. **(f)** Altered dikes: TOP: Contact zone of Dike-2 (0.1–20 g/t Au), black biotite + titanite + epidote in pink albite, minor microcline + quartz, no magmatic textures, WMD-33, 175.8 m; BOTTOM: quartz vein with pink microcline selvages, outer chlorite after biotite in porphyritic Dike-3, WMD-33, 139.3 m

replacement partly overprints magmatic textures at both contacts. Accessory sericite + calcite selectively replace plagioclase, and chlorite + epidote ± pyrite replace biotite.

In the open pit, large parts of this dike were mined as ore (3–20 g/t Au; Fig. 12c). Endoskarn at both contacts, discontinuous and 0.5–5 cm thick, was composed of albite-oligoclase, minor diopside, actinolite, stilpnomelane, titanite, and pyrite (5–10%). Native gold was concentrated at the endoskarn replacement front. Elsewhere, the dike margins were altered in broad zones to a texture-destructive, light red albite-biotite assemblage (Fig. 13f) characterized by a distinct increase in CIPW normative albite + anorthite relative to orthoclase in least-altered microgranite (Table 3). The plagioclase was partly replaced by sericite + calcite, and the biotite by chlorite, epidote, and titanite-magnetite-pyrite aggregates. Trace magnetite and pyrite (0.5% each) were evenly disseminated. Native gold was enclosed in alteration albite and located at quartz-plagioclase grain boundaries (Bucci et al. 2002). The interior of the dike was mottled pink-grey due to dispersed hematite. Pink feldspar replacement bands and quartz-epidote veinlets surrounded by red selvages crosscut the inner part. Pegmatite segregations 5–40 cm thick were abundant in zones up to 4 m wide. In its hanging wall, Dike-2 was associated with a 10-m-wide network of thin, foliation-discordant exoskarn veins mineralized with magnetite, pyrite, pyrrhotite, tellurobismuthite, and native gold. Common vein types were hornblende-quartz, diopside-albite-quartz, actinolite-albite-quartz, and scheelite-molybdenite dated by a Re-Os model age of 2621 ± 10 Ma (Bucci et al. 2002, 2004).

Dike-3 This dike, located below the pit floor west of Dike-2, limits the amphibolite-hosted ore body at depth (Fig. 12b). In the ore skarn, the gold grades in Dike-3 vary from 0.2 to 11.8 g/t. At depth, where the dike merges into a single structure, they reach maximum values of 0.10–0.35 g/t but are mostly < 0.01 g/t Au. The least-altered dike consists of grey biotite microgranite with zoned plagioclase phenocrysts, locally cut be pink replacement veins of granular microcline and quartz (Fig. 13f). It contains 10–20 cm thick pegmatite pods, and rare disseminated magnetite and pyrite. At the intrusive contacts and in cross-cutting bands, potassic alteration is overprinted by grey endoskarn composed of granoblastic albite (80 vol%), calcite (1%), epidote, chlorite-titanite aggregates, and disseminated pyrite and pyrrhotite (2–3%). Late fractures are lined with pyrite, calcite, and quartz (Mueller 1997c).

Discussion

Most LCT pegmatites in the Yilgarn Craton belong to the albite-spodumene subtype, and require a pressure of 300–400 MPa to crystallize spodumene + quartz (London 1984). This pressure equates to a crustal depth of 11–15 km given an average density of 2.7 g/cm^3 and lithostatic load (Spear 1993), implying erosion down to the granite batholith level. In the Southern Cross, Mt Marion-Wattle Dam, and the Pioneer Dome mining districts, LCT pegmatites are spatially associated with gold skarn and skarn-quartz vein deposits, which formed at the same time and at the same depth. The pegmatites and gold deposits are genetically related to a suite of continental-margin I-type biotite granites. Most are post-orogenic (2.65–2.62 Ga) with respect to the last folding phases in the western part of the Eastern Goldfields province, the youngest Archean orogen in the craton (Witt et al. 2020; Mueller et al. 2020).

I-type versus S-type fertile granites

Rare-metal pegmatites belonging to the Li-Cs-Ta (LCT) family may be related to either S- or I-type granites (Cerný et al. 2005). In the Yilgarn Craton, most of the fertile granites are mildly peraluminous, and fractionated pegmatites characterized by Mn-almandine + muscovite are strongly corundum-normative (Table 1), criteria commonly used to infer an S-type origin for the granite-pegmatite suite (Wise et al. 2022). Many biotite granites, however, qualify as I-type magnetite-series by Fe_2O_3/FeO ratio and indicator minerals (magnetite + titanite ± allanite), in particular the K-feldspar megacrystic Wave Rock pluton, the source of hydrothermal magnetite-pyrite mineralization in adjacent orthogneiss. Even the spodumene pegmatites at Mt Marion contain accessory magnetite (Smith and Ross 2017). The zoned Nevoria peraluminous pegmatite-granite intrusion, in contrast, has a low magnetic signature because most of the magnetite and ilmenite were destroyed during sub-solidus alteration. The abundance of secondary rutile (Mueller et al. 2004) suggests ilmenite > magnetite pointing to an ilmenite-series character. However, the absence of magmatic cordierite is critical evidence against an S-type classification (White et al. 1986). Instead, the granite-pegmatite complexes at the continental-margin of the Eastern Goldfields orogen resemble the I-type granites in the Sierra Nevada batholith at the convergent margin of western North America, which display increasing degrees of crustal contamination going east (White et al. 1986; Ague and Brimhall 1987, 1988). The granitic melts emplaced west of the EG orogen clearly interacted with older orthogneiss and with lower continental crust, as indicated by the age spectrum of zircon xenocrysts (ESM Table 3).

In contrast to the LCT pegmatites, the genetic relationship of the Yilgarn gold skarns to the same granite suite relies on the combination of spatial, chronological, and isotopic evidence. A magmatic origin of the high-T gold-bearing fluids is supported by the carbon isotope composition of calcite-rich ore at Marvel Loch (mean fluid $d^{13}C_{PDB} = -4.8‰$;

Mueller et al. 1991b), and by the initial $^{87}Sr/^{86}Sr$ ratios in hydrothermal scheelite (Fig. 14). The highest skarn-related Sr-isotope ratios match those of the local post-orogenic granites. The trend to lower values in source-distal skarns is due to fluid interaction with the greenstone host rocks. The initial isotope ratios of both the gold skarns and I-type granites are distinctly higher than the ratios of mesothermal sericite/biotite gold deposits in the crustal-scale Boulder-Lefroy Fault of the EG orogen, which are associated with mantle-derived porphyries (Mueller et al. 2020).

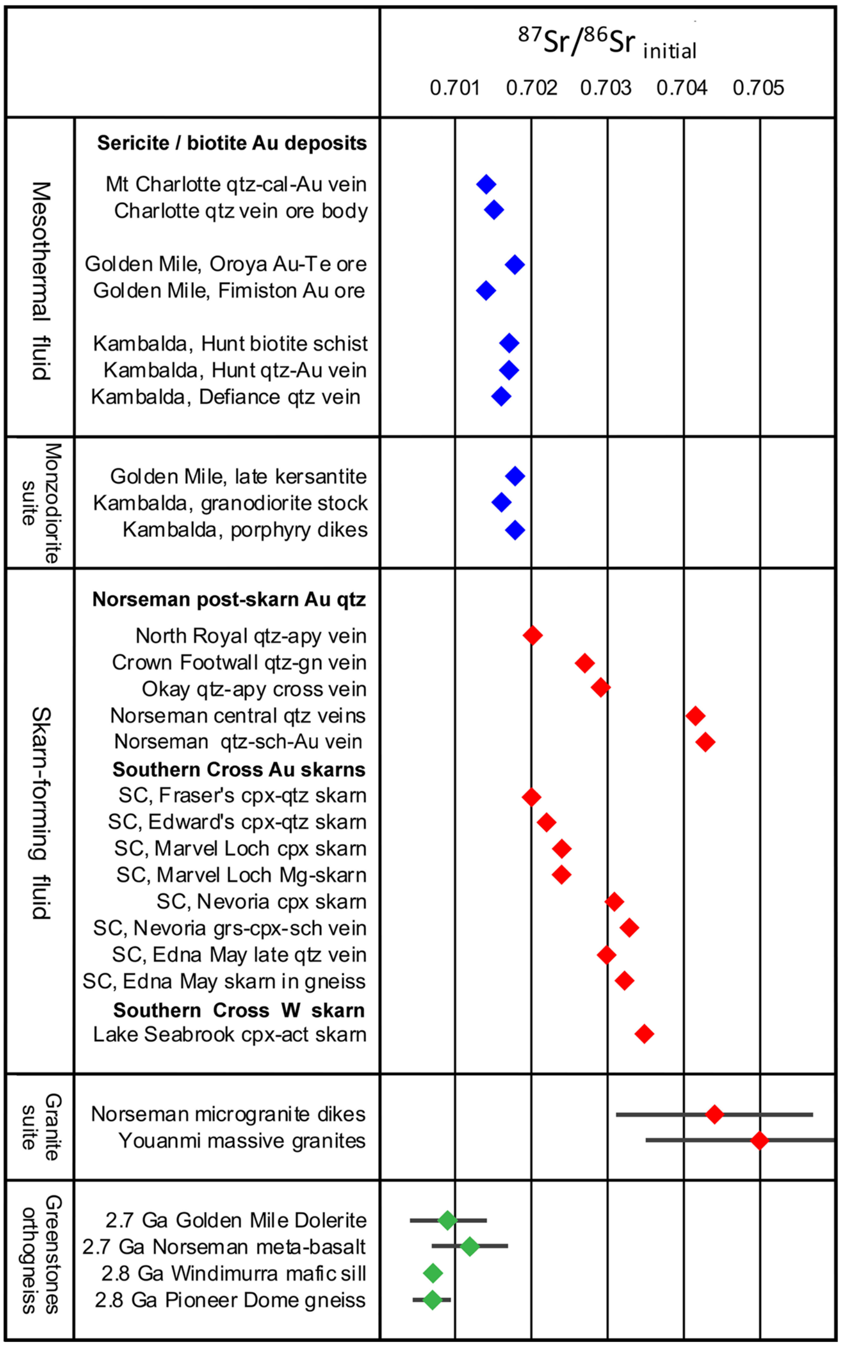

Fig. 14 Strontium isotope composition (± 1-sigma error) of the hydrothermal fluid based on the initial $^{87}Sr/^{86}Sr$ ratios in scheelite from mesothermal gold deposits in the Kalgoorlie / Kambalda districts, skarn-quartz vein deposits in the Norseman district, Kalgoorlie Terrane, and gold and tungsten skarn deposits in the Southern Cross greenstone belt, Youanmi Terrane, Yilgarn Craton. The ratios of granite-greenstone source rocks are based on the measurement of Rb-free magmatic minerals or on the Y-axis intercept of Rb-Sr regression analysis. Data: Mueller et al. (1991a), ESM Table 1

The granite-pegmatite-gold association

The association of granitic pegmatites with gold skarn and quartz vein deposits has also been observed in the Archean Kaapvaal, Slave, Superior and Dharwar cratons, South Africa, Canada and India, respectively, and in the 1.4-1.0 Ga Kibaran fold belt in east Africa (Pohl et al. 2013; Lehmann et al. 2014). Representative high-T gold deposits in these Archean cratons are discussed below. They all contain scheelite, locally in by-product quantities as in the megacrystic diopside skarn of the New Consort mine (1.2% WO_3; MJ Tomkinson, personal communication 1990). The sulfide assemblage is dominated by pyrrhotite + arsenopyrite, associated with loellingite or pyrite, and with Bi-tellurides and native bismuth.

New Consort The New Consort deposit (8 g/t Au; >70 t Au 1886–2020) in the 3.5 Ga Barberton greenstone belt, Kaapvaal Craton, South Africa, comprises skarn stratabound to the folded contact of the Onverwacht meta-komatiite-amphibolite succession with Fig Tree meta-greywacke. The contact is marked by a quartz-phlogopite ± fuchsite-microcline zone (Consort Bar), and dips at moderate angles SSE beneath a broad greywacke synform (Voges 1986; Tomkinson and Lombard 1990; Otto et al. 2007; Kolb et al. 2015). Skarn was mined to 1.7 km vertical depth, and includes diopside-actinolite-scapolite ± garnet-vesuvianite, actinolite-phlogopite-quartz ± calcite, hornblende-biotite-plagioclase-microcline, and retrograde serpentine ± magnetite replacement in the amphibolite-facies volcanic rocks. The hanging-wall meta-greywacke is altered to biotite-rich gneiss containing metasomatic almandine, hornblende, cummingtonite, and retrograde chlorite. Spodumene-albite-quartz pegmatites with holmquistite selvages were emplaced at the mineralized contact and into NNW-striking faults, which offset the stratabound ore (Tomkinson and Lombard 1990; Otto et al. 2007). Skarn titanite U-Pb (3027 ± 7.5 Ma) and pegmatite Rb-Sr (3040 ± 84 Ma) ages suggest that the pegmatite-skarn association may be related to late intrusions in the Nelspruit granite batholith north of the mine (3106 ± 3 Ma; Kolb et al. 2015).

Lupin The Lupin deposit at Contwoyto Lake (9.6 g/t Au; >100 t Au 1982–2002), Slave Craton, Canada, consists of reduced hedenbergite-hornblende skarn stratabound to folded grunerite-quartz BIF interbedded with 2.7 Ga meta-greywacke (Lhotka and Nesbitt 1989, 1990; Geusebroek and Duke 2004). The ore bodies persist without change in mineralogy to 1.4 km depth. The deposit is located in the greenschist to amphibolite facies aureole of the post-tectonic, 2.60–2.58 Ga Contwoyto Lake batholith (Yamashita et al. 1999). The cordierite-in isograd in greywacke is located 500 m north of the mine at surface but intersects the shaft at the 550 m level implying a 45° south dip. The appearance of cordierite coincides with that of muscovite-tourmaline pegmatite dikes linked to the batholith (Geusebroek and Duke 2004). The batholith is composed of biotite granodiorite and granite, locally muscovite-sillimanite-bearing, and contains pegmatite bodies and disseminated magnetite + pyrite (Bostock 1980).

Musselwhite The Mussewhite deposit at Opapimiskan Lake (7–9 g/t Au; >124 t Au 1997–2013), Superior Craton, Canada, consists of almandine-cummingtonite-hornblende skarn stratabound to grunerite-quartz-magnetite BIF intercalated with a 3.0 Ga amphibolite-metakomatiite volcanic succession (Hall and Rigg 1986; Biczok et al. 2012; McNicoll et al. 2016). The tabular to pipe-shaped ore bodies are controlled by tight folds plunging 20–35° north. The Sm-Nd age of gold-related garnet (2690 ± 9 Ma) is bracketed by the monazite U-Pb ages of local peraluminous granite dikes (2716 ± 2 Ma to 2669 ± 1 Ma; Biczok et al. 2012). LCT pegmatite dikes were intersected by drill holes beneath the ore bodies in an area measuring 6 × 4 km. They consist of quartz and albite, lesser K-feldspar, muscovite, tourmaline, spessartine, spodumene and lepidolite, and accessory apatite, fluorite, Ta-Nb oxides, gahnite and uraninite (Taylor and Henham 2002). Both Musselwhite and Lupin are similar in structural setting and skarn mineralogy to the Nevoria deposit (Mueller 1997a).

James Bay The Éléonore deposit (6.1 g/t Au; >142 t Au reserves in 2016) east of James Bay, Superior Craton, comprises stratabound zones of quartz-actinolite-diopside skarn, and skarn-and/or quartz-tourmaline banded phlogopite-microcline gneiss and phlogopite-amphibole schist (Ravenelle et al. 2009; Fontaine et al. 2017). The ore zones dip steeply east and replace amphibolite-facies meta-greywacke (<2675 Ma). Late- to post-tectonic leucogranite and pegmatite dikes (2620−2603 Ma), some mineralized with gold and others crosscutting, are associated with the ore bodies (Fontaine et al. 2017).

The Cheechou deposit (0.65 g/t Au; 60 t Au resources in 2020) is located 15 km southeast of Éléonore at the margin of an ilmenite-series granodiorite pluton dated at 2612 ± 1 Ma (Fontaine et al. 2017; Turlin et al. 2022). The mineralized margin of the pluton is pervasively altered to quartz-albite and quartz-feldspar-diopside ± actinolite assemblages, and intruded by sheeted late- to post-kinematic pegmatite dikes with local actinolite-feldspar selvages. Quartz, diopside-actinolite, scheelite, gold and sulfides occur disseminated, in veinlets, and enclosed in tourmaline-bearing pegmatite (mostly pyrite). Chlorite ± epidote-pyrite-gold veinlets are late-stage (Turlin et al. 2022). Mineralization (5–49 g/t Au) in meta-greywacke at the contact of the altered pluton southwest and west of Cheechou is associated with gold- and sulfide-bearing pegmatites (Fontaine et al. 2017). LCT pegmatites are not recognized in the Éléonore and Cheechou mine areas but are explored for spodumene on the Shaakichiuwaanaan (Patriot Battery Metals 2025) and Adina properties to the north (Winsome Resources 2024). The Cheechou deposit resembles the endoskarn in syn-gold granite dikes at the Chalice deposit described above.

Kolar The Kolar deposit (16 g/t Au; 810 t Au 1880–2001) in the 2.9 Ga Kolar greenstone belt, Dharwar Craton, India, consists of quartz reefs and sheeted veins enclosed in zoned diopside-hornblende-biotite skarn bound to the sheared lithologic contacts of amphibolite and meta-komatiite (Narayanaswami et al. 1960; Hamilton and Hodgson 1986). More than 90% of all production came from the Champion quartz-reef system (1% sulfides, mainly galena), and from the Oriental sulfide lode (10% pyrrhotite + arsenopyrite). The mineralized sheared contacts strike north, dip 40–60° west on the upper mine levels but steepen to sub-vertical at depth. They are displaced by NNW-striking, steeply dipping faults spaced in a zone 2.5 km wide. Where the N- and NNW-striking shear zones intersect, thick gold-quartz veins form drag folds defining high-grade shoots, and wall-rock alteration is intense (Hamilton and Hodgson 1986). The Champion reef-system was mined over a strike of 8 km and down to 3.2 km vertical depth. Tourmaline-bearing muscovite-garnet pegmatites increase in abundance below 2 km depth, where they crosscut but are also parallel to auriferous veins. Some contain gold and sulfides (Safonov et al. 1984). They may be related to the Closepet granite suite dated at 2.55–2.50 Ga (Srinivasa Sarma et al. 2011). The Kolar deposit shows striking similarities in structural setting and quartz vein sulfide-telluride mineralogy to Au-Ag deposits in the Norseman district (Mueller 1992).

Skarn versus hypozonal orogenic gold

The high-T gold deposits discussed above are "skarn deposits" in the sense of Einaudi and Burt (1982), given the distinctive calcic or magnesian gangue and the inclusion of native gold in silicates. In most of the studies quoted, they are interpreted as "hypozonal orogenic", a term implying the formation in crustal-scale shear zones at > 12 km depth, broadly synchronous with amphibolite-facies metamorphism (Groves et al. 1998; Ridley et al. 2000; Goldfarb et al. 2005). Moreover, "Au skarns in regional metamorphic terranes" are regarded as transitional to the non-magmatic orogenic group because they "share a lack of association with igneous activity" (Meinert et al. 2005: 323–324).

Apart from New Consort and Musselwhite, Kaapvaal and Superior cratons, the space-time association of gold skarn deposits with LCT pegmatites has been established in three mining districts of the east-central Yilgarn Craton, where radiometric dating also confirmed a link between high-T skarn formation (650–450 °C) and granite-pegmatite emplacement, in particular at Nevoria and Chalice. The skarns do not share the high Au: Ag ratio (> 5:1) typical of orogenic deposits. Bulk ore Au: Ag ratios vary from 3:1 to 1:1 and may change to silver-dominant, if post-skarn quartz veins are present (Au: Ag = 1:5).

Most Archean gold skarns are stratabound to sheared lithologic contacts but are not controlled by crustal-scale faults. At Southern Cross, the offsets at skarn-altered contacts are < 200 m, often much less, certainly not on the scale of 12 km as at the gold-rich Boulder-Lefroy Fault in the Eastern Goldfields orogen (Mueller et al. 2020). There is no genetic relationship to metamorphic grade. The km-wide amphibolite-facies aureole of the Ghooli Dome batholith is 2772 ± 5 Ma old (U-Pb metamorphic zircon), whereas the Corinthian and Nevoria gold skarns in this aureole are dated at 2620 ± 6 Ma and 2636 ± 1 Ma, respectively. At Nevoria, post-skarn faults control mesothermal sericite-chlorite-carbonate alteration, which lacks sulfides and gold but occurs at the same crustal level as the offset gold skarn.

Many Archean skarns display features typical of Phanerozoic reduced tungsten skarns, which are associated with pegmatitic I-type granites emplaced at 6–10 km depth (150–250 MPa) at continental margins (Einaudi et al. 1981; Newberry 1998). In contrast to the silicate host rocks of the Archean skarns, the tungsten skarns replace marble with interbeds of hornfels. Scheelite-bearing prograde skarn (600–450 °C) composed of grossular-andradite with > 20 mol% almandine + spessartine and hedenbergite (Newberry 1983), is overprinted by retrograde (450–350 °C) hornblende-chlorite and biotite-plagioclase assemblages rich in pyrrhotite. Bulk ore from the Cantung and MacTung skarns in northwestern Canada contains 1.04–1.13% W, 0.25–0.49% Cu, 530–1000 g/t Bi and 0.7–1.9 g/t Au (Newberry 1998). Hydrous parts of the Cantung skarn are enriched in electrum, native bismuth, Bi-tellurides, and Bi-Te selenides (Lentz et al. 2017).

The Cretaceous Sandong deposit (75,000 t WO_3+Au; 1947–1992) in South Korea illustrates the down-temperature evolution of infiltration skarn to the quartz-vein stage, similar to the evolution in gold deposits of the Norseman and Kolar districts. At Sandong, prograde skarn (600–400 °C; 0.1–0.3% WO_3) in marble evolved from an oxidized grossular-andradite-diopside to a reduced grossular-spessartine-hedenbergite assemblage overprinted by inner hydrous skarn (400–300 °C; 0.5–3.0% WO_3). A Stage 1 hornblende zone with disseminated magnetite and pyrrhotite grades into a Stage 2 biotite-muscovite-chlorite zone with a high density of quartz veins and minor molybdenite, pyrrhotite, pyrite, bismuthinite, tetradymite, and native gold (John 1963; Seo et al. 2017; Kang et al. 2022).

Metamorphic versus magmatic H_2O-CO_2 fluids

Aqueous-carbonic fluids (X_{H2O} = 0.80–0.95; $X_{CO2\ [\pm CH4,\ H2S]}$ = 0.05–0.20) of metamorphic orogin are an essential part of the orogenic model for gold-only deposits, as discussed in Goldfarb and Pitcairn (2023). These authors argue against a role for magmatic H_2O-CO_2 fluids below a crustal depth of about 6 km. However, the solubility of CO_2 in hydrous felsic melts strongly increases with pressure, and the exsolution of an increasingly CO_2-rich aqueous fluid is to be expected as crustal depth increases, too (Ridley and Diamond 2000; Blundy 2022). Quartz-hosted melt inclusions in volcanic rocks related to the 23 Ma Pine Grove porphyry molybdenum deposit in Utah contain 6–8 wt% H_2O and up to 960 ppm CO_2. Calculated saturation pressures as high as 430 MPa require that volatile exsolution began at 16 km depth during magma ascent (Lowenstern 2001).

The 1.7 Ga Harney Peak peraluminous granite, emplaced at about 13 km depth (350 MPa) into the Proterozoic metamorphic basement of the Black Hills, South Dakota, is surrounded by a wide field of LCT pegmatites. Aplite and pegmatite layers in the 2-mica granite are characterized by tourmaline, accessory Mn-almandine, apatite, monazite, and sillimanite (Nabelek and Ternes 1997). Primary inclusions in tourmaline and quartz trapped a magmatic H_2O-$CO_2 \pm CH_4$ fluid of variable X_{CO2} (0.03–0.57; mode 0.2), low to moderate salinity (0–11 wt% $NaCl_{eq}$), and bulk density (0.62–0.91 g/cm^3) at >450–500 °C (Nabelek and Ternes 1997). In the zoned Jiajika pegmatite field, China, Be-rich pegmatites close to the source granite contain primary inclusions of an intermediate density, supercritical H_2O-CO_2 fluid (T_h = 335–354 °C, 20–30 vol% CO_2, 3.2–5.1 wt% $NaCl_{eq}$) trapped at pressures of 314–424 MPa. The assemblage spodumene + quartz prevails in outer pegmatites (Wang et al. 2023).

In the Yilgarn Craton, the diffusion of hydrothermal fluid from LCT pegmatites into the country rock is evident at Greenbushes and Mt Marion given holmquistite in the host amphibolites. Mass transfer on a much larger scale from granite into marble is inferred for the scheelite-bearing skarns in the Sierra Nevada batholith, California, where fluid conditions are estimated at 150–200 MPa, 450–650 °C, X_{CO2} = < 0.1 to 0.2, and salinities of 4–8 wt% $NaCl_{eq}$ (Einaudi et al. 1981). The Nevoria gold skarn deposit in the Southern Cross greenstone belt, Yilgarn Craton, shares the low to moderate salinity H_2O-CO_2 fluid characteristic of peraluminous granites, LCT pegmatites, and deep-seated reduced tungsten skarns. At Nevoria, the reduction of a magmatic H_2O-CO_2 fluid, evident in the CO_2 / CH_4 ratio, was probably responsible for the restriction of economic gold grades to the ferrous BIF (30 wt% FeO).

Conclusions

1) In the Yilgarn Craton, Western Australia, and in other Archean cratons worldwide, gold skarn deposits characterized by their high-T (650-450°) magnesian or calcic silicate gangue are associated in space and time with post-orogenic granite-pegmatite complexes, in particular with LCT pegmatites. In the Yilgarn Craton, the fertile suite of peraluminous granites and fractionated pegmatites varies from I-type magnetite- to ilmenite-series, dependent on the degree of crustal contamination.
2) The Archean spodumene pegmatites and the gold skarn deposits formed at a crustal depth of 11–15 km (300–400 MPa) in a batholithic environment deeper than that of Phanerozoic reduced tungsten skarns (150–250 MPa). The skarns postdate the amphibolite-facies aureole metamorphism in the host greenstone belts by up to 150 million years. They are stratabound to sheared lithologic contacts of limited displacement (< 200 m), and are not controlled by crustal-scale faults.
3) Most gold skarn deposits are associated with fractionated granite-pegmatite complexes or with microgranite porphyry dikes. Some intrusions are altered to endoskarn, others are albitized, and some contain sulfides and native gold. Where both skarn and intrusion have been dated, the radiometric ages agree within error but the local dikes may be pre-, syn- and post-gold, related to multiple intrusive activity below the deposit. At Kolar, India, ore bodies extend 3.2 km away from their granitic source.
4) In the reducing environment of the greenstone belt, gold precipitated during prograde skarn formation at high fluid temperatures (650-450°C) from near-critical, low to moderate salinity H_2O-CO_2 fluids identical in composition to those trapped in fertile peraluminous granites, LCT pegmatites, and deep-seated Phanerozoic tungsten skarns. Mass balances and zonation patterns indicate that the infiltrating fluid introduced CO_2, Ca, Mg, K and sulfur apart from Au, Ag, Bi and W. Most ore skarns are characterized by lower Au:Ag ratios (3:1 to 1:1) than orogenic deposits (>5:1). Where post-skarn quartz veins are present, the ore may contain more silver than gold (e.g., Norseman Au:Ag = 1:5).
5) In the outer parts of Archean skarn systems, subcalcic amphiboles, cordierite, and biotite are part of the alteration assemblage in aluminous metamorphic rocks (amphibolite, gneiss). In some cases, late-stage sodic gedrite assemblages (Wattle Dam) or main-stage anthophyllite-albite fels (Ghost Crab; 550±50°C) constitute gold ore in a broader skarn zone. Sodium enrichment may increase late or in distal parts of the ore skarn away from the source pluton. Alternatively, it may be related to the type of subsolidus alkali metasomatism in the intrusion. The Ghost Crab deposit is located close to the >200 m thick Mt Marion albite-spodumene pegmatite complex. A common granitic source, however, has not been identified and should be the subject of future research.

Supplementary Information The online version contains supplementary material available at https://doi.org/10.1007/s00126-025-01361-z.

Acknowledgements The author thanks editor-in-chief Bernd Lehmann for his invitation to submit this paper. His suggestions and those of two anonymous referees helped to improve the manuscript significantly. He is grateful to Larry Meinert for his introduction to skarn geology during his PhD study at the University of Western Australia, and to Marco Einaudi for sharing his knowledge on skarns and other intrusion-related ore deposits. Greg Hall deserves special mention for his long-standing support.

Funding Open Access funding enabled and organized by Projekt DEAL.

Data availability All data used are accessible in the manuscript and in the Electronic Supplementary Material (ESM).

Declarations

Conflict of interest The author declares no conflict of interest.

References

Ague JJ, Brimhall GH (1987) Granites of the batholiths of California: products of local assimilation and regional-scale crustal contamination. Geology 15:63–66

Ague JJ, Brimhall GH (1988) Regional variations in bulk chemistry, mineralogy, and the composition of mafic and accessory minerals in the batholiths of California. Geol Soc Amer Bull 100:891–911

Ahmat AL (1986) Metamorphic patterns in the greenstone belts of the Southern Cross Province, Western Australia. Geol Surv Western Australia, Prof Paper 19: 1–21

Alacer Gold (2012) South Kalgoorlie Operations, NI 43–101 Technical Report No. 129510300-REP-R0001-00. Australian stock exchange ASX, March 2012. http://www.sedar.com

Andrews PB (1975) Spargoville nickel deposits. In: Knight CL (ed) Economic geology of Australia and Papua New Guinea. Aust Inst Min Metall Monogr 5: 89–91

Barley ME, Brown SJA, Krapez B, Kositcin N (2008) Physical volcanology and geochemistry of a late Archaean volcanic arc: Kurnalpi and Gindalbie Terranes, Eastern Goldfields superterrane, Western Australia. Precambrian Res 161:53–76

Barth TFW (1955) Presentation of rock analyses. J Geol 63:348–363

Bath AB, Walshe JL, Cloutier J, Rotherham J, Hutchison R, Holleneck E, Verrall M, Schmitt L (2020) Alteration patterns linked to high-grade gold mineralization at the Wattle Dam deposit, Western Australia. Ore Geol Rev 125:1–16

Batt GE, Crook D, Brand N, Kerr S (2021) Agile management and long-term strategy in exploration: the 'lucky' discovery of the Sinclair pollucite deposit, Eastern Goldfields, Western Australia. Aust J Earth Sci 68:684–696

Bettenay LF (1977) Regional geology and petrogenesis of Archaean granitoids in the southeastern Yilgarn Block, Western Australia. Dissertation, the University of Western Australia, Perth, 238 p

Bickle MJ, Archibald NJ (1984) Chloritoid and staurolite stability: implications for metamorphism in the Archaean Yilgarn block, Western Australia. J Metam Geol 2:179–203

Biczok J, Hollings P, Klipfel P, Heaman L, Maas R, Hamilton M, Kamo S, Friedman R (2012) Geochronology of the North Caribou greenstone belt, Superior Province Canada: implications for tectonic history and gold mineralization at the Musselwhite mine. Precambrian Res 192–195:209–230

Blatchford T, Honman CS (1917) The geology and mineral resources of the Yilgarn Goldfield: part III. The gold belt north of Southern Cross including Westonia. Geol Surv West Australia Bull 71:1–321

Blight DF, Compston W, Wilde SA (1981) The Logue Brook granite: age and significance of deformation zones along the Darling scarp. Geol Surv West Australia Annual Report for 1980, pp 72–80

Bloem EJM, Dalstra HJ, Groves DI, Ridley JR (1994) Metamorphic and structural setting of Archaean amphibolite-hosted gold deposits near Southern Cross, Southern Cross Province, Yilgarn block, Western Australia. Ore Geol Rev 9:183–208

Blundy J (2022) Chemical differentiation by mineralogical buffering in crustal hot zones. J Petrol 63:1–36

Bohlen SR, Montana A, Kerrick DM (1991) Precise determinations of the equilibria kyanite-sillimanite and kyanite-andalusite and a revised triple point for Al_2SiO_5 polymorphs. Am Mineral 76:677–680

Bostock HH (1980) Geology of the Itchen Lake area, district of Mackenzie. Can Geol Surv Mem 391:1–101

Bucci LA, Hagemann SG, Groves DI, Standing JG (2002) The Archean Chalice gold deposit: a record of complex, multistage, high-temperature hydrothermal activity and gold mineralization associated with granitic rocks in the Yilgarn craton, Western Australia. Ore Geol Rev 19:23–67

Bucci LA, McNaughton NJ, Fletcher IR, Groves DI, Kositcin N, Stein HJ, Hagemann SG (2004) Timing and duration of high-temperature gold mineralization and spatially associated granitoid magmatism at Chalice, Yilgarn craton, Western Australia. Econ Geol 99:1123–1144

Bucher K, Frey M (2002) Petrogenesis of metamorphic rocks, 7th edn. Springer, Berlin, 341 p

Cassidy KF, Champion DC, Krapez B, Barley ME, Brown SJA, Blewett RS, Groenewald PB, Tyler IM (2006) A revised geological framework for the Yilgarn craton, Western Australia. Geol Surv West Australia Record 2006/8:1–8

Cerný P, Meintzer RE (1988) Fertile granites in the Archean and Proterozoic fields of rare-element pegmatites: crustal environment, geochemistry and petrogenetic relationships: In: Taylor RP, Strong DF (eds) Recent advances in the geology of granite-related mineral deposits. Can Inst Min Metall Spec Vol 39: 170–207

Cerný P, Blevin PL, Cuney M, London D (2005) Granite-related ore deposits. Econ Geol 100th Anniversary, pp 337–370

Chappell BW, White AJR (2001) Two contrasting granite types: 25 years later. Aust J Earth Sci 48:489–499

Chen SF, Riganti A, Wyche S, Greenfield JE, Nelson DR (2003) Lithostratigraphy and tectonic evolution of contrasting greenstone successions in the central Yilgarn craton, Western Australia. Precambrian Res 127:249–266

Chin RJ, Smith RA (1983) Explanatory notes, 1:250,000 geological map, sheet SH 50–12, Jackson, Western Australia. Geol Surv West Australia, 30 p

Chin RJ, Hickman AH, Thom R (1984) Explanatory notes, 1:250,000 geological map, sheet SI 50– 4, Hyden, Western Australia. Geol Surv West Australia, 21 p

Corona Resources (2020) Resource estimate update for the Spargo's Reward project, Eastern goldfields, Western Australia, February 26, 2020. http://www.coronaresources.com.au

Cox R, Tyrwhitt DS (1975) Pioneer nickel prospects, near Norseman. In: Knight CL (ed) Economic geology of Australia and Papua New Guinea. 1. Metals. Aust Inst Min Metall Monogr 5: 79–81

Crook DJ, Kerr ST, Booth JA, Brand NW, Panting R (2019) The discovery and geology of Sinclair, Australia's first caesium deposit. ASEG Ext Abstr 2019:1–5. https://doi.org/10.1080/22020586.2019.12072971

Dalstra HJ (1995) Metamorphic and structural evolution of greenstone belts of the Southern Cross-Diemals region of the Yilgarn Block, Western Australia, and its relationship to gold mineralization. Dissertation, the University of Western Australia, Perth, 219 p

Dalstra HJ, Bloem EJM, Ridley JR, Groves DI (1998) Diapirism synchronous with regional deformation and gold mineralization, a new concept for granitoid emplacement in the Southern Cross Province, Western Australia. Geol Mijnbouw 76:321–338

Einaudi MT, Burt DM (1982) Terminology, classification, and composition of skarn deposits. Econ Geol 77:745–754

Einaudi MT, Meinert LD, Newberry RJ (1981) Skarn deposits. Econ Geol 75th Anniversary Vol, 317–391

Ernst WG (1968) Amphiboles. Minerals, rocks and inorganic materials. Monograph series of theoretical and experimental studies, vol 1. Springer, Berlin, 125 p

Fan HR, Groves DI, Mikucki EJ, McNaughton NJ (2000) Contrasting fluid types at the Nevoria gold deposit in the Southern Cross greenstone belt, Western Australia: implications of auriferous fluids depositing ores within an Archean banded iron-formation. Econ Geol 95:1527–1536

Fehlberg B, Giles CW (1984) Archaean volcanic exhalative gold mineralization at Spargoville, Western Australia. In: Foster RP (ed) Gold'82: the geology, geochemistry and genesis of gold deposits. Balkema, Rotterdam, pp 285–303

Fontaine A, Dubé B, Malo M, Ravenelle J-F, Fournier E, McNicoll V, Beausoleil C, Prud'homme N, Goutier J (2017) The Éléonore gold mine: Exploration, discovery and understanding of an emerging gold district in Eeyou Istchee James Bay, Superior Province, northern Québec, Canada. In: Tschirhart V, Thomas MD (eds) Proceedings of Exploration 17: Sixth decennial international conference on mineral exploration, pp 601–617

Future Battery Minerals Ltd (2025) Kangaroo Hills and Miriam lithium projects, ASX:FBM. https://futurebatteryminerals.com.au/Coolgardie

Gee RD (1982) Explanatory notes, 1:250,000 geological map, sheet SH 50– 16, Southern cross, Western Australia. Geol Surv West Australia

Geusebroek PA, Duke NA (2004) An update on the geology of the Lupin gold mine, Nunavut, Canada. Explor Min Geol 13:1–13

Goldfarb RJ, Pitcairn I (2023) Orogenic gold: is a genetic association with magmatism realistic? Miner Deposita 58:5–35

Goldfarb RJ, Baker T, Dubé B, Groves DI, Hart CJR, Gosselin P (2005) Distribution, character, and genesis of gold deposits in metamorphic terranes. Econ Geol 100th Anniversary, pp 407–450

Groves DI, Goldfarb RJ, Gebre-Mariam M, Hagemann SG, Robert F (1998) Orogenic gold deposits: a proposed classification in the context of their crustal distribution and relationship to other deposit types. Ore Geol Rev 13:7–27

Hall RS, Rigg DM (1986) Geology of the West Anticline Zone, Musselwhite prospect, Opapimiskan Lake, Ontario, Canada. In: Macdonald AJ (ed) Proceedings of Gold'86, an International Symposium on the Geology of Gold, pp 124–136

Hamilton JV, Hodgson CJ (1986) Mineralization and structure of the Kolar gold field, India. In: Macdonald AJ (ed) Proceedings of Gold'86, an international Symposium on the Geology of Gold, 270–283

Hancock W, Ramsden AR, Taylor GF, Wilmshurst JR (1971) Some ultramafic rocks of the Spargoville area, Western Australia. Geol Soc Aust, Spec Publ 3: 269–280

Hagemann SG, Cassidy KF (1999) Archean high-P-T, granitoid-hosted gold mineralization at Westonia, Western Australia: II. P-T-X constraints on a gold-bearing paleohydrothermal system in a high-grade terrain. In: Mineral Deposits – Processes to Processing. Proc Fifth Biennial SGA Conference, London

Holland TJB, Powell R (1998) An internally consistent thermodynamic data set for phases of petrological interest. J Metam Geol 16:309–343

Hunter WM (1988) Yilmia 1:100,000 map sheet 3135, 1st edition. Geol Surv Western Australia

Ishihara S (1981) The granitoid series and mineralization. Econ Geol 75th Anniversary Vol:458–484

John YW (1963) Geology and origin of Sandong tungsten mine, Republic of Korea. Econ Geol 58:1285–1300

Kalamazoo Resources (2024) Kali metals find more high-grade lithium in the Higginsville district: Spargoville project, Flynn-Giles / Green flame soil anomaly. Australian stock exchange (ASX) statement, February 2024. http://www.kzr.com.au

Kang J, Choi S-G, Seo J, Kim S-T, Kim G-B, Cho S-J, Lee G, Lee YJ (2022) A genetic model of the giant Sandong W-Mo skarn deposit in the Taebaeksan basin, South Korea. Ore Geol Rev 150:105187

Keats W (1991) Geology and gold mines of the Bullfinch-Parker range region, Southern Cross Province, Western Australia. Geol Surv West Australia Rept 28:1–44

Kidman Resources (2017) The Mt Holland project. http://kidmanresources.com.au/live/wp-content/uploads/2016/08/Twinings-Au-Longsection-January-2017.png

Kolb J, Dziggel A, Bagas L (2015) Hypozonal lode gold deposits: A genetic concept based on a review of the new consort, Renco, Hutti, Hira Buddini, Navachab, Nevoria and the Granites deposits. Precambrian Res 262:20–44

Krapez B, Brown SJA, Hand J, Barley ME, Cas RAF (2000) Age constraints on recycled crustal and supracrustal sources of Archaean metasedimentary sequences, Eastern Goldfields Province, Western Australia: evidence from SHRIMP zircon dating. Tectonophysics 322:89–133

Lehmann B, Halder S, Munana JR, de la Paix Ngizimana J, Biryabarema M (2014) The geochemical signature of rare-metal pegmatites in central Africa: magmatic rocks in the Gatumba tin-tantalum mining district, Rwanda. J Geochem Expl 144:528–538

Lentz CPE, McFarlane CRM, Falck H (2017) Physiochemical controls on gold mineralization in the Amber Zone at the Cantung mine, N.W.T. Mineral resources to discover– 14th SGA Biennial Meeting 2017, Quebec City, Ext Abstr 1: 315–318

Lhotka PG, Nesbitt BE (1989) Geology of unmineralized and gold-bearing iron-formation, Contwoyto Lake - Point Lake region, Northwest Territories, Canada. Can J Earth Sci 26:46–64

Lhotka PG, Nesbitt BE (1990) Relationship of calc-silicate rocks to gold mineralization in the Lupin deposit, N.W.T., Canada. In: Hausen DM, Halbe DN, Petersen EU, Tafuri WJ (eds) Gold'90 Symposium, Salt Lake City, Utah. Soc Min Metall Expl, pp 123–134

Libby JW, Groves DI, Vearncombe JR (1991) The nature and tectonic significance of the crustal-scale Koolyanobbing shear zone, Yilgarn craton, Western Australia. Aust J Earth Sci 38:229–245

London D (1984) Experimental phase equilibria in the system $LiAlSiO_4$-SiO_2-H_2O: a petrogenetic grid for lithium-rich pegmatites. Am Mineral 69:995–1004

Lowenstern JB (2001) Carbon dioxide in magmas and implications for hydrothermal systems. Miner Deposita 36:490–502

Magnetic Resources NL (2010) Mt Vernon iron ore targets. Australian stock exchange ASX:MAU release, 16 March 2010. https://magres.com.au
Matheson RS, Miles KR (1947) The mining groups of the Yilgarn goldfield north of the Great Eastern railway. Geol Surv West Australia Bull 101:227–242
Maximus Resources (2024) Mining news select conference, March 2024. Australian stock exchange ASX presentation. www.maximusresources.com
McNicoll V, Dubé B, Castonguay S, Oswald W, Biczok J, Mercier-Langevin P, Skulski T, Malo M (2016) The world-class Musselwhite BIF-hosted gold deposit, Superior Province, Canada: new high-precision U-Pb geochronology and implications for the geological setting of the deposit and gold exploration. Precambrian Res 272:133–149
Meinert LD, Dipple GM, Nicolescu S (2005) World skarn deposits. Economic Geology 100th Anniversary, pp 299–336
Miller M, McLeod R, Devlin S (1999) Discovery of the Ghost Crab deposit, Kalgoorlie, Western Australia. In: Vinar J (ed) New generation gold mines 99, case histories of discovery. Perth, Conference Proceedings, pp 127–141
Miyano T, Klein C (1989) Phase equilibria in the system K_2O-FeO-MgO-Al_2O_3-SiO_2-H_2O-CO_2 and the stability limit of stilpnomelane in metamorphosed Precambrian iron formations. Contr Mineral Petrol 102:478–491
Mueller AG (1991) The Savage Lode magnesian skarn in the Marvel Loch gold-silver mine: Southern Cross greenstone belt, Western Australia: part I. Structural setting, petrography and geochemistry. Can J Earth Sci 28:659–685
Mueller AG (1992) Petrogenesis of amphibole-biotite-calcite-plagioclase alteration and laminated gold-silver quartz veins in four Archean shear zones of the Norseman district, Western Australia. Can J Earth Sci 29:388–417
Mueller AG (1997a) The Nevoria gold skarn deposit in Archean iron-formation, Southern Cross greenstone belt, Western Australia: I. Tectonic setting, petrography, and classification. Econ Geol 92:181–209
Mueller AG (1997b) Petrography of the Ghost Crab gold deposit, Norseman-Wiluna greenstone belt, Western Australia. Perth, unpublished company report, 75 p
Mueller AG (1997c) Petrography of gold skarn and granite intrusions at the Chalice deposit, Norseman-Wiluna greenstone belt, Western Australia. Perth, unpublished company report, 66 p
Mueller AG, McNaughton NJ (2000) U-Pb ages constraining batholith emplacement, contact metamorphism, and the formation of gold and W-Mo skarns in the Southern Cross area, Yilgarn craton, Western Australia. Econ Geol 95:1231–1257
Mueller AG, de Laeter JR, Groves DI (1991a) Strontium isotope systematics of hydrothermal minerals from epigenetic Archean gold deposits in the Yilgarn Block, Western Australia. Econ Geol 86:780–809
Mueller AG, Groves DI, Delor CP (1991b) The Savage Lode magnesian skarn in the Marvel Loch gold-silver mine, Southern Cross greenstone belt, Western Australia: part II. Pressure-temperature estimates and constraints on fluid sources. Can J Earth Sci 28:686–705
Mueller AG, Campbell IH, Schiotte L, Sevigny JH, Layer PW (1996) Constraints on the age of granitoid emplacement, metamorphism, gold mineralization, and subsequent cooling of the Archean greenstone terrane at Big Bell, Western Australia. Econ Geol 91:896–915
Mueller AG, Nemchin AA, Frei R (2004) The Nevoria gold skarn deposit, Southern Cross greenstone belt, Western Australia: II. Pressure-temperature-time path and relationship to postorogenic granites. Econ Geol 99:453–478
Mueller AG, Hagemann SG, McNaughton NJ (2020) Neoarchean orogenic, magmatic and hydrothermal events in the Kalgoorlie-Kambalda area, Western Australia: constraints on gold mineralization in the Boulder Lefroy-Golden Mile fault system. Miner Deposita 55:633–663
Nabelek PI, Ternes K (1997) Fluid inclusions in the Harney Peak granite, Black Hills, South Dakota, USA: implications for magmatic solubility and evolution of magmatic volatiles and crystallization of leucogranite magmas. Geochim Cosmochim Acta 61:1447–1465
Narayanaswami S, Ziauddin M, Ramachandra AV (1960) Structural control, and localization of gold-bearing lodes, Kolar goldfield, India. Econ Geol 55:1429–1459
Nemchin AA, Pidgeon RT (1997) Evolution of the Darling Range batholith, Yilgarn craton, Western Australia. J Petrol 38:625–649
Newberry RJ (1983) The formation of subcalcic garnet in scheelite-bearing skarns. Can Mineral 21:529–544
Newberry RJ (1998) W- and Sn-skarn deposits: A 1998 status report. In: Lentz DR (ed) Mineralized intrusion-related skarn systems. Mineral Ass Can, Short Course 26: 289–335
Otto A, Dziggel A, Kisters AFM, Meyer FM (2007) The New Consort gold mine, Barberton greenstone belt, South Africa: orogenic gold mineralization in a condensed metamorphic profile. Miner Deposita 42:715–735
Partington GA (1990) Environment and structural controls on the intrusion of the giant rare metal Greenbushes pegmatite, Western Australia. Econ Geol 85:437–456
Partington GA (2017) Greenbushes tin, tantalum and lithium deposit. In: Phillips GN (ed) Australian ore deposits. Aust Inst Min Metall Monogr 32: 153–157
Partington GA, McNaughton NJ, Williams IS (1995) A review of the geology mineralization, and geochronology of the Greenbushes pegmatite, Western Australia. Econ Geol 90:616–635
Patriot Battery Metals Inc (2025) Patriot announces discovery of a large cesium zone at Shaakichiuwaanaan. Australian Stock Exchange ASX:PMT announcement March 3, 2025. https://www.patriotbatterymetals.com
Perring CS, Golding SD, Hallberg JA (1990) Felsic porphyries. In: Ho SE, Groves DI, Bennett JM (eds) Gold deposits of the Archaean Yilgarn Block, Western Australia: Nature, genesis and exploration guides. Univ Western Austr, Geol Dept Univ Extension 20: 114–127
Phelps-Barber Z, Trench A, Groves DI (2022) Recent pegmatite-hosted spodumene discoveries in Western Australia: insights for lithium exploration in Australia and globally. Appl Earth Sci 131:100–113
Pioneer Resources Ltd (2020) Evaluation of Sinclair caesium mine Stage 2 underway. Australian stock exchange ASX:PIO announcement 8 June 2020
Pohl WL, Biryabarema M, Lehmann B (2013) Early Neoproterozoic rare metal (Sn, Ta, W) and gold metallogeny of the central Africa region: a review. Appl Earth Sci (Trans Inst Min Metall B) 122:66–82
Powell R, Holland TJB (1994) Optimal geothermometry and geobarometry. Am Mineral 79:120–133
Qiu YM (1997) Long-lived granitoid magmatism in the Southern Cross Province, Yilgarn Craton, Western Australia, and its relationship to Archaean lode-gold mineralization. Dissertation, the University of Western Australia, Perth
Qiu YM, McNaughton NJ (1999) Source of Pb in orogenic lode-gold mineralization: Pb isotope constraints from deep crustal rocks from the southwestern Archaean Yilgarn craton, Australia. Miner Deposita 34:366–381
Qiu YM, McNaughton NJ, Groves DI, Dalstra HJ (1999) Ages of internal granitoids in the Southern Cross region, Yilgarn craton, Western Australia, and their crustal evolution and tectonic implications. Aust J Earth Sci 46:971–981
Ramelius Resources (2012) Deep diamond drilling at the Wattle Dam north project EIS, government co-funded drilling grant reference number DAG2012/00043752, Coolgardie mineral field, Western Australia. Report December 2012, 20 p: https://geodocs.dmirs.wa.gov.au/Web/documentlist/10/Report_Ref/A96373
Ravenelle J-F, Dubé B, Malo M, McNicoll V, Nadeau L (2009) Geology of the amphibolite-facies world-class Roberto gold deposit,

Eleonore property, James Bay, Canada. In: Williams PJ et al (eds) Smart science for exploration and mining. Proc Tenth Biennial SGA Meeting, Townsville, pp 59–61

Richardson SW, Gilbert MC, Bell PM (1969) Experimental determination of the kyanite-andalusite and andalusite-sillimanite equilibria: the aluminum silicate triple point. Am J Sci 267:259–272

Ridley JR, Diamond LW (2000) Fluid chemistry of lode-gold deposits and implications for genetic models. In: Hagemann SG, Brown P (eds), Gold in 2000. Rev Econ Geol 13: 141–162

Ridley JR, Groves DI, Knight JT (2000) Gold deposits in amphibolite and granulite facies terrains of the Archean Yilgarn craton, Western Australia: evidence and implications of syn-metamorphic mineralisation. In: Marshall B, Vokes FM (eds) Metamorphic and metamorphogenic ore deposits. Rev Econ Geol 11: 265–290

Safonov YG, Genkin AG, Vasudev VN, Krishna Rao B, Anantha Iyer GV (1984) Genetic features of gold ore deposits at Kolar, Dharwar craton, India. J Geol Soc India 25:145–154

Sciuba M, Beaudoin G, Grzela D, Makvandi S (2020) Trace element composition of scheelite in orogenic gold deposits. Miner Deposita 55:1149–1172

Seifert F (1970) Low-temperature compatibility relations of cordierite in haplopelites of the system K_2O-MgO-Al_2O_3-SiO_2-H_2O. J Petrol 11:73–99

Seo JH, Yoo BC, Villa IM, Lee JH, Lee T, Kim C, Moon KJ (2017) Magmatic-hydrothermal processes in Sandong W-Mo deposit, Korea: study of fluid inclusions and ^{39}Ar-^{40}Ar geochronology. Ore Geol Rev 91:316–334

Smith B, Ross J (2017) Mount Marion lithium pegmatite deposit. In: Phillips GN (ed) Australian ore deposits. Aust Inst Min Metall Monogr 32: 161–162

Spear FS (1993) Metamorphic phase equilibria and pressure-temperature-time paths. Mineral Soc Am Monogr 1–799

Spray JG (1986) Geological setting of Archaean vein-type gold deposits within the Norseman greenstone sequence, Western Australia. In: Gallagher MJ, Ixer RA, Neary CR, Pritchard HM (eds) Metallogeny of basic and ultrabasic rocks. Inst Min Metall London, pp 133–150

SQM, Sociedad Quimica y Minera de Chile (2022) Technical report summary: Mt. Holland lithium project, April 2022. http://q4live.s25.clientfiles.s3-website-us-east-1.amazonaws.com/757756353/files/doc_news/2022/4/25/96.2-Mt-Holland-Technical-Report-Summary.pdf

Srinivasa Sarma D, Fletcher IR, Rasmussen B, McNaughton NJ, Ram Mohan M, Groves DI (2011) Archean gold mineralization synchronous with late cratonization of the western Dharwar craton, India: 2.52 Ga U-Pb ages of hydrothermal monazite and xenotime in gold deposits. Miner Deposita 46:273–288

Steiger RH, Jäger E (1977) Subcommission of geochronology: convention of the use of decay constants in geo- and cosmochronology. Earth Planet Sci Lett 36:359–362

Swager CP, Griffin TJ, Witt WK, Wyche S, Ahmat AL, Hunter WM, McGoldrick PJ (1995) Geology of the Archaean Kalgoorlie terrane– An explanatory note. Geol Surv West Australia Rep 48:1–26

Sweetapple MT, Grigson MW, Tornatora P, Urgine S (2019) The Archean Mt. Cattlin spodumene pegmatite group and 3D geochemical mapping of large unzoned pegmatites of economic significance. Can Mineral 57:803–805

Takagi T, Tsukimura K (1997) Genesis of oxidized- and reduced-type granites. Econ Geol 92:81–86

Taylor RP, Henham R (2002) The nature and distribution of tantalum-bearing minerals in newly discovered, rare-element pegmatites at the Musselwhite mine, northwestern Ontario. Explor Min Geol 10:85–93

Thern ER, Nelson DR (2012) Detrital Zircon age structure within ca. 3 Ga metasedimentary rocks, Yilgarn Craton: Elucidation of Hadean source terranes by principal component analysis. Precambrian Res 214–215:28–43

Thomas A, Johnson K, MacGeehan PJ (1990) Norseman gold deposits. In: Hughes FE (ed) Geology of the mineral deposits of Australia and Papua New Guinea. Aust Inst Min Metall Monogr 14: 493–504

Tomkinson MJ, Lombard A (1990) Structure, metamorphism and mineralization in the New Consort gold mine, Barberton greenstone belt, South Africa. In: Glover JE, Ho SE (eds) Third International Archean Symposium, Perth, 1990, Ext Abstr, pp 377–379

Turlin F, De Souza S, Jébrak M, Groulier P-A, Turcotte J (2022) Vein topology, structures, and distribution during the prograde formation of an Archean gold stockwork. Geol Soc Am Bull 134:815–831

Villa IM, De Bièvre P, Holden NE, Renne PR (2015) IUPAC-IUGS recommendation on the half life of ^{87}Rb. Geochim Cosmochim Acta 164:382–385

Voges FD (1986) The New Consort gold mine, Barberton greenstone belt. In: Anhaeusser CR, Maske S (eds) Mineral deposits of Southern Africa 1:163–168

Wang G-G, Zheng F-B, Ni P, Wu Y-W, Qi W-X, Li Z-A (2023) Fluid properties and ore-forming process of the giant Jiajika Li deposit, Western China. Ore Geol Rev 160:105613

Watkins KP, Hickman AH (1990) Geological evolution and mineralization of the Murchison Province, Western Australia. Geol Surv West Australia Bull 137:1–267

White AJR, Clemens JD, Holloway JR, Silver LT, Chappell BW, Wall VJ (1986) S-type granites and their probable absence in southwestern North America. Geology 14:115–118

Whitney DL, Evans BW (2010) Abbreviations for names of rock-forming minerals. Am Mineral 95:185–187

Wiedenbeck M, Watkins KP (1993) A time scale for granitoid emplacement in the Archean Murchison Province, Western Australia, by single zircon geochronology. Precambrian Res 61:1–26

Wilkins RWT, Davidson LR, Ross JR (1970) Occurrence and infrared spectra of holmquistite and hornblende from Mt Marion, near Kalgoorlie, Western Australia. Contr Min Petrol 28:280–287

Williamson HC, Barr DJ (1965) Gold mineralization in the Yilgarn goldfield. In: McAndrew J (ed) Geology of Australian ore deposits. 8th Commonwealth Mining and Metallurgical Congress, Australia and New Zealand, 87–94

Winsome Resources Ltd (2024) Adina mineral resource increases 33% to 78 Mt at 1.15% Li_2O with 79% indicated. Australian Stock Exchange ASX:WR1 release 28 May 2024. http://www.winsomeresources.com.au

Wise MA, Müller A, Simmons WB (2022) A proposed new mineralogical classification system for granitic pegmatites. Can Mineral 60:229–248

Witt WK (1992) Heavy-mineral characteristics, structural settings, and parental granites of pegmatites in Archaean rocks of the eastern Yilgarn craton. Geol Surv West Australia Rec 1992/10:1–54

Witt WK, Cassidy KF, Lu Y-J, Hagemann SG (2020) The tectonic setting and evolution of the 2.7 Ga Kagoorlie-Kurnalpi rift, a world-class Archean gold province. Miner Deposita 55:601–631

Yamashita K, Creaser RA, Stemler JU, Zimaro TW (1999) Geochemical and Nd-Pb isotopic systematics of late Archean granitoids, southwestern Slave Province, Canada: constraints for granitoid origin and crustal isotopic structure. Can J Earth Sci 36:1131–1147

Zenith Minerals Ltd (2024) Lithium Forward Program 2024. Australian Stock Exchange release ASX: ZNC. http://www.zenithminerals.com.au

Publisher's note Springer Nature remains neutral with regard to jurisdictional claims in published maps and institutional affiliations.